Remote Sensing of Environment 226 (2019) 74–92

Contents lists available at ScienceDirect

Remote Sensing of Environment

journal homepage: www.elsevier.com/locate/rse

Long-term continuity in land surface phenology measurements: A comparative assessment of the MODIS land cover dynamics and VIIRS land surface phenology products

Minkyu Moon[a,*], Xiaoyang Zhang[b,c], Geoffrey M. Henebry[d,e], Lingling Liu[b,c], Josh M. Gray[f], Eli K. Melaas[a], Mark A. Friedl[a]

[a] Department of Earth and Environment, Boston University, Boston, MA 02215, USA
[b] Geospatial Sciences Center of Excellence, South Dakota State University, Brookings, SD 57007, USA
[c] Department of Geography, South Dakota State University, Brookings, SD 57007, USA
[d] Department of Geography, Environment, and Spatial Sciences, Michigan State University, East Lansing, MI 48824, USA
[e] Center for Global Change and Earth Observations, Michigan State University, East Lansing, MI 48823, USA
[f] Department of Forestry and Environmental Resources, North Carolina State University, Raleigh, NC 27695, USA

ARTICLE INFO

Keywords:
Land surface phenology
VIIRS
MODIS
Phenology product
Comparison
Validation

ABSTRACT

Vegetation phenology contributes to, and is diagnostic of, seasonal variation in ecosystem processes and exerts important controls on land-atmosphere exchanges of carbon, water, and energy. Satellite remote sensing provides a valuable source of data for monitoring the phenology of terrestrial ecosystems and has been widely used to map geographic and interannual variation in land surface phenology (LSP) over large areas. The Visible Infrared Imaging Radiometer Suite (VIIRS) land surface phenology product provides global data sets characterizing the annual LSP of terrestrial ecosystems, and is designed to support long-term continuity of LSP measurements from the Moderate Resolution Imaging Spectroradiometer (MODIS). We used data from VIIRS and MODIS to evaluate the agreement and characterize the similarities and differences between LSP data from each instrument. Specifically, we compare data from the Collection 6 MODIS Land Cover Dynamics (LCD) product with data from the newly developed VIIRS LSP product over the most common land cover types in North America. To do this, we assessed the overall agreement between time series of vegetation indices from VIIRS and MODIS, evaluated the correspondence between retrieved phenometrics from each instrument, and analyzed sources of differences between phenometrics from the each product. As part of this analysis, we also compared phenometrics from MODIS and VIIRS with phenometrics derived from Landsat Analysis Ready Data and PhenoCam time series. Results show that two-band enhanced vegetation index (EVI2) values from VIIRS and MODIS are similar ($R^2 > 0.81$; root mean square deviation < 0.062), but that VIIRS EVI2 time series show more high frequency variation than time series from MODIS. Further, even though the VIIRS and MODIS products are generated using different instruments and algorithms, phenometrics from each product are similar and show only minor differences within and across land cover types. Systematic differences between phenometrics from the two products were generally less than one week (absolute bias 4.8 ± 3.0 days), and RMSDs were less than two weeks for most phenometrics across different land cover classes (10.7 ± 4.3 days). Comparison of VIIRS and MODIS LSP data with corresponding metrics estimated from Landsat and PhenoCam data consistently showed high agreement among the data sets. Overall, results from this analysis indicate that the VIIRS LSP product provides excellent continuity with the MODIS record. However, studies attempting to create high-fidelity long-term LSP time series by merging these products should exploit the overlap period of MODIS and VIIRS to estimate land cover-specific corrections for modest systematic bias in the MODIS LCD product relative to the VIIRS LSP product.

* Corresponding author at: 685 Commonwealth Avenue, Boston, MA 02215, USA.
E-mail addresses: moon.minkyu@gmail.com, mkmoon@bu.ed (M. Moon).

https://doi.org/10.1016/j.rse.2019.03.034
Received 10 October 2018; Received in revised form 18 February 2019; Accepted 24 March 2019
0034-4257/ © 2019 Elsevier Inc. All rights reserved.

1. Introduction

Phenology is an important functional attribute of terrestrial ecosystems and is widely used as a diagnostic indicator of climate change impacts on ecosystem properties and processes (Richardson et al., 2013). In particular, green leaf phenology regulates a number of important surface biophysical properties and processes including land surface albedo (Moore et al., 1996; Ollinger et al., 2008), surface energy budgets (Dorman and Sellers, 1989; Ryu et al., 2008), the partitioning of surface radiation between latent and sensible heat fluxes (Hogg et al., 2000; Schwartz, 1992), and aerodynamic and surface resistances (Blanken and Black, 2004; Zhao et al., 2016). Therefore, accurate representation of spatiotemporal dynamics in vegetation phenology is important for a variety of topics in both basic and applied ecological sciences ranging from monitoring the impact of climate change on species and communities, to modeling seasonal variation in ecosystem processes (Chen et al., 2016; Menzel et al., 2006; Peñuelas et al., 2009; Richardson et al., 2010).

Prior to the era of Earth observation satellites, observations of vegetation phenology were collected via field surveys, which recorded the timing of discrete phenological events for individual species, such as flowering and leaf emergence in spring and leaf coloration and leaf drop in fall (e.g., Caprio, 1957). These data continue to be collected and have substantial value. However, because field surveys generally focus on a limited set of plants and species at the local scale, generalizing and upscaling results from field data (e.g., to the scale of entire biomes) is challenging. In the last several decades, satellite remote sensing has been shown to provide a powerful complement to field observations that can be used to monitor and characterize the nature, magnitude, and timing of changes in land surface phenology at regional to global scales. Because of its 30+ year record of measurements, the Advanced Very High Resolution Radiometer (AVHRR) has been widely used for this purpose (Buitenwerf et al., 2015; Dardel et al., 2014; de Beurs and Henebry, 2005; Fang et al., 2001; Fensholt and Rasmussen, 2011; Guay et al., 2014). However, the coarse spatial resolution of AVHRR data, in combination with uncertainty in radiometric calibration, low quality snow and cloud detection, broad spectral channels, and errors in geolocation introduce considerable uncertainty to time series of vegetation indices and phenological metrics derived from this instrument (Gutman, 1999; Ju and Masek, 2016; Nagol et al., 2009; Sulla-Menashe et al., 2018; White et al., 2009).

The Moderate Resolution Imaging Spectroradiometer (MODIS) onboard NASA's Terra (since 1999) and Aqua (since 2002) platforms have provided high quality global imagery at 250, 500, and 1 km spatial resolution that is well-suited for retrieving land surface phenology (Ganguly et al., 2010; Zhang et al., 2003). In particular, the MODIS Land Cover Dynamics (LCD) product (MCD12Q2) provides annual measurements of global land surface phenology at 500 m spatial resolution and has been successfully used to explore a variety of climate-ecosystem relationships at large spatial scales (Friedl et al., 2014; Hufkens et al., 2012; Keenan et al., 2014; Zhang et al., 2004). However, the MODIS sensors are well-beyond their original design life and are expected to cease operation in the coming years. To provide continuity with both MODIS and AVHRR, the Visible Infrared Imaging Radiometer Suite (VIIRS) was launched in October 2011 as a part of the instrument suite onboard the Suomi National Polar-Orbiting Partnership (NPP). With the launch of the first Joint Polar Satellite System (JPSS-1) in November of 2017, VIIRS provides the operational basis for long-term continuity of the MODIS land product suite (Justice et al., 2013). In support of this vision, a new operational land surface phenology (LSP) product has been developed based on VIIRS data (Zhang et al., 2018b) and is designed to provide long-term continuity with the MODIS LCD product.

Because the VIIRS LSP and MODIS LCD products are derived from different instruments and are based on different algorithms, differences in the data products are unavoidable. To evaluate the similarities and differences between these two data products and, more specifically, to address the question of whether the VIIRS product provides continuity with the MODIS product for long-term studies of land surface phenology, here we present a systematic comparison of the Collection 6 MODIS LCD product (Gray et al., 2019) and the newly developed VIIRS LSP product (Zhang et al., 2018b). Several studies have previously examined correspondence between satellite-based LSP metrics and both in-situ measurements of phenology (Ganguly et al., 2010; Liang et al., 2011; Zhang et al., 2006) and other proxies of vegetation phenology such as time series of gross primary productivity derived from flux networks (Melaas et al., 2013; Park et al., 2016; Sakamoto et al., 2010). Preliminary assessment of the overall accuracy of the VIIRS LSP product is presented elsewhere (Zhang et al., 2017b, 2018a). Here we focus on a product-to-product comparison, and specifically address the question of whether the VIIRS and MODIS products can be used jointly for studies that require time series of land surface phenology measurements. To do this, we systematically compared the operational VIIRS LSP and MODIS LCD products across the Contiguous United States (CONUS) and Eastern Canada, focusing on three sub-regions that span a wide range of climate and land cover types in the Northeastern United States, Eastern Canada, the Central U.S, and the Southwestern U.S. Our analysis includes three elements. First, we assessed the agreement between phenophase transition metrics (hereafter, phenometrics; e.g., the timing of greenness increase onset) from each product. Second, we conducted a comprehensive evaluation to attribute differences between the two products to (1) differences in MODIS versus VIIRS input data and their associated quality, and (2) differences in the algorithm used to generate each product. Third, we conducted a multi-scale comparison of the MODIS LCD and VIIRS LSP products against phenometrics derived from Landsat (Melaas et al., 2016) and from the PhenoCam Dataset V1.0 (Richardson et al., 2018a).

2. Data and methods

2.1. Overview of land surface phenology product algorithms

To provide context for the analyses and results we describe below, we first provide an overview of the MODIS LCD and VIIRS LSP products, focusing on their primary similarities and differences. Specifically, there are three main steps in each land surface phenology algorithm: (1) preprocessing of vegetation index time series to remove spurious values, (2) time series smoothing or model fitting to create continuous time series without gaps, and (3) identification of phenometrics (Fig. 1). Space does not allow for a complete description of each algorithm. For more detailed information, please see Zhang et al. (2018b) and Gray et al. (2019).

Both products use daily nadir bidirectional reflectance distribution function (BRDF)-adjusted reflectance (NBAR) products (VNP43IA4 for VIIRS and MCD43A4 for MODIS) to compute time series of the two-band enhanced vegetation index (EVI2; Jiang et al., 2008) at each pixel, which serves as the primary input to both algorithms (Fig. 1a). Note that the MODIS NBAR product is produced using MODIS observations from both Terra and Aqua; whereas, the VIIRS NBAR product is generated using VIIRS observations only from Suomi NPP. Spurious EVI2 values caused by snow-contamination are replaced by “background values”, which represent the minimum snow-free EVI2 at each pixel (Zhang et al., 2006). To reduce data volumes, daily NBAR data are sampled every 3 days in the VIIRS LSP algorithm, while in the MODIS LCD algorithm daily NBAR data are sampled every 5 days. Both products use snow flags included as part of the NBAR product (VNP43IA2 for VIIRS and MCD43A2 for MODIS) from each instrument to identify snow-contaminated values. The VIIRS product also uses land surface temperature as an additional constraint (Zhang et al., 2018b), while the MODIS product uses the normalized-difference snow index (NDSI) to

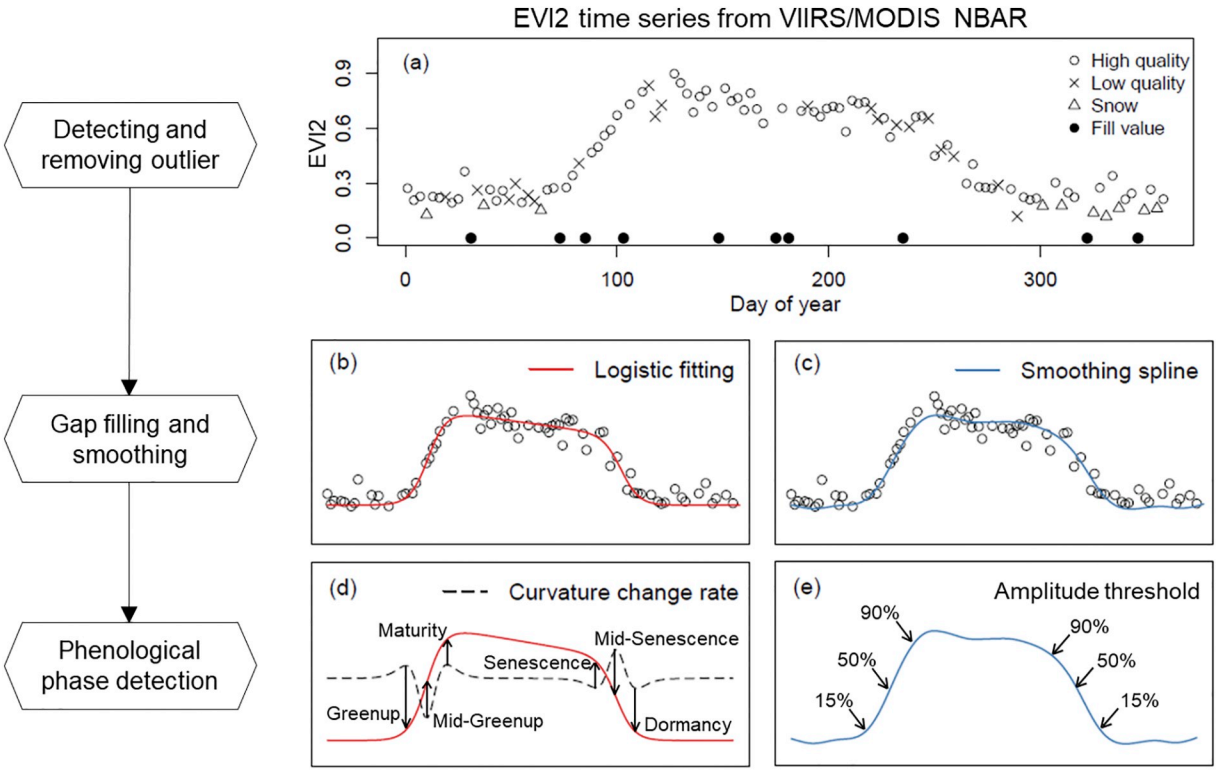

Fig. 1. Schematic of the algorithms used to create the VIIRS LSP and MODIS LCD products. Panel (a) is a sample of VIIRS EVI2 time series for a single pixel. Panels (b) and (d) illustrate the VIIRS algorithm, while panels (c) and (e) illustrate the MODIS algorithm.

flag snow-contaminated pixels (Gray et al., 2019).

To create smooth and gap-filled data, the VIIRS LSP algorithm first applies a Savitzky-Golay filter to EVI2 time series. A hybrid piecewise logistic model (HPLM) is then fit to the smoothed time series at each pixel (Fig. 1b). New in Collection 6, the MODIS LCD algorithm removes outliers and generates smoothed EVI2 time series in a single step using penalized cubic splines (Fig. 1c). For the VIIRS LSP, phenometrics are identified using the rate of change in curvature of the fitted HPLM; whereas, the MODIS LCD approach uses prescribed thresholds in the amplitude of variation in EVI2 for each phenological cycle (Fig. 1d and e, respectively). In the VIIRS LSP algorithm two local maxima in the rate of change of curvature during the "green-up" phase are used to identify phenometrics. Specifically, the day of year (DOY) corresponding to each of these maxima identifies the timing of greenup and maturity onset, and the date corresponding to the minimum rate of change in the curvature corresponds to the DOY when EVI2 reaches 50% of its seasonal amplitude. For the MODIS product, the timing of greenup onset, mid-greenup, and maturity onset are retrieved as the DOY when the splined EVI2 time series first crosses 15%, 50%, and 90% of its seasonal amplitude, respectively. In both products, corresponding phenometrics during senescence, or "green-down" (i.e., senescence onset, mid-senescence, and dormancy onset) are identified in a similar manner.

2.2. Intercomparison of land surface phenology products

To compare the two products, we used a stratified random sample of pixels located in three 10° by 10° tiles in North America that encompass a wide range of climate and land cover types (tiles H12V04, H11V04, and H08V05; Fig. 2). In each tile, we identified the three dominant vegetated land cover types based on the Collection 6 MODIS Land Cover Type product (MCD12Q1; Sulla-Menashe et al., 2019). Note, however, that for tile H08V05 (centered over the arid southwestern United States), pixels belonging to the Barren or Sparsely Vegetated class in the MCD12Q1 product, which are defined as having < 10% vegetation cover, were excluded from the evaluation. Previous work has shown that discrepancies between phenometrics derived from VIIRS and MODIS are often associated with the low quality of EVI2 time series (Zhang et al., 2018b). Thus, we excluded pixels where differences in phenometric values between the two products were unusually large (viz., > 90 days). This step resulted in 0–4% of pixels from the original sample being removed from each land cover type in each of the tiles for each phenometric (Table A1). Finally, prior to performing our assessment, we applied a 3 × 3 moving window median filter to each phenometric in each product to account for the fact that the effective spatial resolutions of NBAR data are > 500 m and are different for each sensor (~565 m × 595 m and 833 m × 618 m in the VIIRS and MODIS NBAR products, respectively; Campagnolo et al., 2016).

2.3. Attribution of differences related to sensors versus algorithms

To evaluate and attribute sources of differences between the two products, we performed three sets of analyses. First, because differences in EVI2 time series derived from MODIS versus VIIRS are an obvious source of disagreement, we evaluated the overall agreement and quality of model fits to VIIRS and MODIS NBAR EIV2 time series. To do this, we used a randomly selected set of 10,000 pixels from each of the three dominant land cover types in each of the three tiles included in our analysis. To quantify the agreement between observations and fitted time series, we calculated the growing season agreement index (AI) for all pixels as defined by Zhang et al. (2018b):

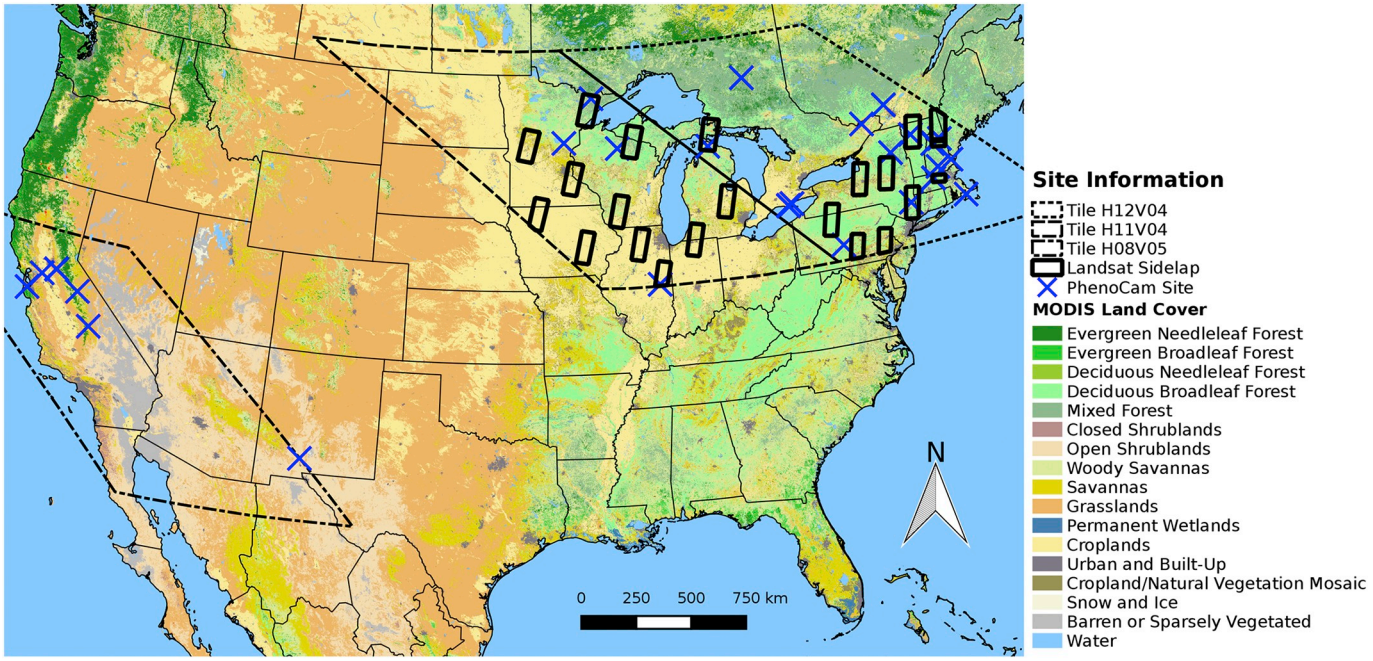

Fig. 2. Map of the study area showing three VIIRS and MODIS tiles (H12V04, H11V04, and H08V05), 22 Landsat sidelap regions, and 34 PhenoCam sites used in the analysis. The background image shows the IGBP land cover type across the study area from the Collection 6 MODIS Land Cover Type product in 2013.

$$AI = 100 - 100\frac{\sum_{i=0}^{n}(P_{(i)} - O_{(i)})^2}{\sum_{i=0}^{n}(\mid P_{(i)} - \bar{O} \mid + \mid O_{(i)} - \bar{O} \mid)^2} \quad (1)$$

where n is the number of observations, $P_{(i)}$ is the modeled value for the ith observation, $O_{(i)}$ is the EVI2 for the ith observation, and $\bar{O}$ is the mean EVI2 across the time series at each pixel. The VIIRS and MODIS products use 3-day and 5-day composites, respectively, to reduce data volumes and noise in EVI2 time series. However, because the purpose of this analysis is to compare the quality of input data for both products, we applied the same criteria for both sources of EVI2 data. Specifically, we used 3-day composited EVI2 values from both MODIS and VIIRS in 2013, selecting either the best quality EVI2 value or the maximum value composite, if more than one high quality value was available in each 3-day period.

Second, we assessed how differences in both input data and algorithms introduce differences in phenometrics from each of the two products. To account for differences in input data, we estimated phenometrics from VIIRS and MODIS NBAR EVI2 time series using the VIIRS LSP algorithm and compared the resulting phenometrics. Then, to assess the contribution of using different algorithms, we applied both VIIRS LSP and MODIS LCD algorithms to MODIS NBAR EVI2 time series. Note that we used MODIS data for this analysis because MODIS EVI2 time series were less noisy than corresponding time series from VIIRS (see Results section), thereby minimizing differences caused by noise in input data.

Third, to provide an assessment of how data-induced uncertainties impact phenometrics, we performed a statistical simulation experiment wherein EVI2 time series and noise were simulated and used to estimate phenometrics. To do this, we first fit logistic models to EVI2 time series and retained the model residuals. We then treated the modeled EVI2 time series as truth and the model residuals as instrument-induced errors, generated simulated EVI2 time series using non-parametric bootstrapping (Efron, 1979), and estimated phenometrics from the simulated EVI2 time series. To do this, we used the same data set of 10,000 randomly selected pixels from each land cover type in each of the tiles described above.

2.4. Comparison with results from the Landsat phenology algorithm

We used results from the Landsat Phenology Algorithm (LPA) described by Melaas et al. (2013, 2016) to provide an independent source of land surface phenology information that could be compared with VIIRS LSP and MODIS LCD results. The LPA exploits the temporal density of observations available in overlap regions between adjacent Landsat scenes (hereafter, “sidelaps”), and provides estimates of the DOY associated with the start and end of the growing season (SOS and EOS, respectively) at 30 m spatial resolution that are equivalent to the mid-greenup and mid-senescence dates from VIIRS and MODIS (Fig. 1). Comparison of LPA results against local-scale in-situ measurements indicate the LPA provides high quality estimates of SOS and EOS, especially for SOS (Melaas et al., 2016).

For this analysis, we generated LPA results using USGS Landsat Analysis Ready Data in 22 sidelaps distributed across the Central and Northeastern U.S (Fig. 2) in 2013 and 2014. This data set includes Landsat 8 imagery, which increases data density, and the LPA implementation used here incorporates the topographic correction described by Tan et al. (2013), which is important in regions where topographically-induced variation in Landsat surface reflectance affects LPA results (E. Melaas, *pers. comm.*). For each sidelap, corresponding values for mid-greenup and mid-senescence dates from the VIIRS LSP and MODIS LCD products were extracted, and data from all three sources were up-scaled to 1500 m spatial resolution (i.e., 3×3500 m pixel windows) using the mean of all available 30 m LPA retrievals and the median of VIIRS LSP and MODIS LCD values in each 1500 m cell. To minimize deviations caused by missing data in LPA retrievals (e.g., caused by clouds), we excluded all 1500 m cells where fewer than 100 LPA SOS or EOS values out of ~2500 pixels were available. To explore how our results varied as a function of geographic variation in

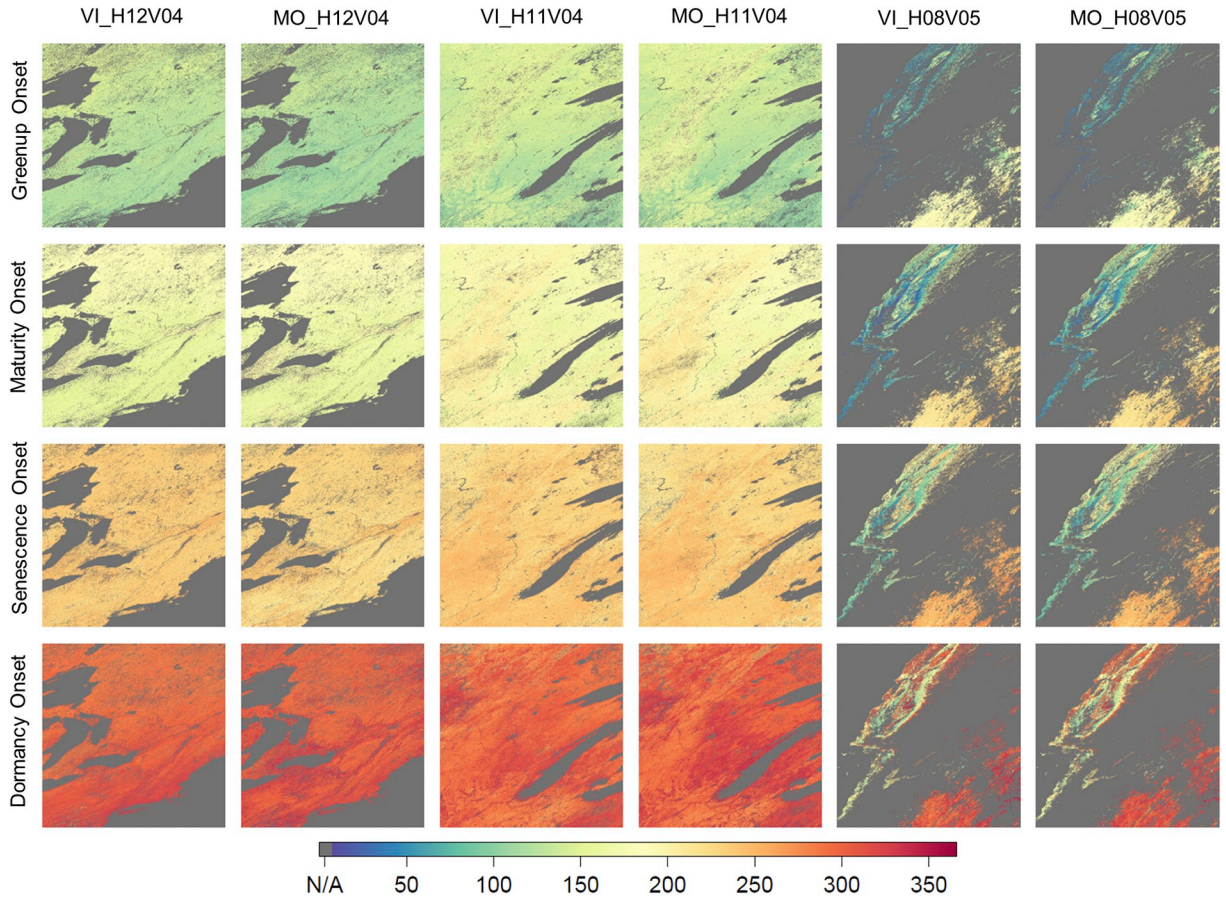

Fig. 3. Images showing the timing of greenup onset, maturity onset, senescence onset, and dormancy onset (day of year) from the VIIRS LSP and the MODIS LCD products in 2013. Each tile is dominated by different land cover types: forests in the Northeastern U.S. and Eastern Canada (H12V04), croplands in the Central U.S. (H11V04), and shrublands and grasslands in the Southwestern U.S (H08V05). In the columns, VI and MO denote the VIIRS and MODIS products, respectively.

ecological conditions, we stratified our analysis based on the EPA level II ecoregions (Omernik, 1987; Omernik and Griffith, 2014).

2.5. Comparison with phenometrics from the PhenoCam dataset V1.0

To provide a second source of independent assessment data, we used phenometrics estimated using time series of PhenoCam imagery. PhenoCam is a continental-scale network that uses near-surface imagery from digital cameras to track vegetation phenology at high temporal resolution (Richardson et al., 2018a). The PhenoCam Dataset V1.0 (Richardson et al., 2018a) includes about 750 site-years of observations that characterize vegetation phenology in all major ecosystems across North America. For this work, we used all PhenoCam site-years for which corresponding VIIRS and MODIS phenometrics were available, again focusing on the date of mid-greenup and mid-senescence. More specifically, we used phenometrics derived from Green Chromatic Coordinate (G_{CC}; Sonnentag et al., 2012) time series corresponding to the date when G_{CC} values reach 50% of their seasonal amplitude during the greenup and green-down periods for each site-year. For this comparison, we only used data from the sites where the vegetation type of the region of interest in PhenoCam imagery corresponded to the MODIS land cover type surrounding the PhenoCam site. Specifically, sites where > 5 pixels within 3 × 3500 m windows centered over the site had land cover labels that were different from the PhenoCam vegetation type were excluded from the analysis. The resulting data set included 34 sites and a total 109 phenometrics (53 and 56 site-years for SOS and EOS, respectively; Table A2). In addition, to illustrate some of the challenges associated with comparison of results from data streams with such different spatial resolutions, we also present a comparison of G_{CC} and EVI2 time series (and corresponding phenometrics) at the Jasper Ridge PhenoCam site.

3. Results

3.1. Baseline comparison of the VIIRS LSP and MODIS LCD products

To evaluate the overall agreement between the VIIRS LSP and MODIS LCD products, Fig. 3 shows maps of phenometrics derived from the VIIRS LSP and MODIS LCD products in 2013 for each of the three tiles included in our analysis. Table 1 presents statistics summarizing the agreement between phenometrics derived from each product (stratified by land cover type). Fig. 4 shows scatterplots illustrating agreement between phenometrics for the two products. Fig. 5 presents year-to-year agreement from 2013 to 2014 in the bias and RMSD between VIIRS LSP and MODIS LCD phenometrics. Overall, results indicate that phenometrics were in close agreement across land cover types, with phenometrics corresponding to the mid-point in the greenup and green-down periods (mid-greenup and mid-senescence) showing the strongest agreement. The maximum difference in mean phenometrics was less than two weeks in woody savannas in temperate regions (cf., tiles H12V04 and H11V04). In general, however, mean values across the study region and all six phenometrics showed

Table 1
Summary statistics (mean, $\bar{x}$, and standard deviation, σ) for each tile, stratified by the three dominant land cover types from Fig. 3, excluding barren and sparsely vegetated pixels. IGBP land cover was derived from the Collection 6 MODIS Land Cover Type product: 4: deciduous broadleaf forests; 5: mixed forests; 7: open shrublands; 8: woody savannas; 9: savannas; 10: grasslands; 12: croplands.

Tile ID	IGBP	%	Product	Greenup onset		Date at mid-greenup		Maturity onset		Senescence onset		Date at mid-senescence		Dormancy onset	
				$\bar{x}$	σ	$\bar{x}$	σ	$\bar{x}$	σ	$\bar{x}$	σ	$\bar{x}$	σ	$\bar{x}$	σ
Forests	5	32	VIIRS	131	12	152	10	173	12	232	12	260	8	289	11
			MODIS	122	12	149	9	174	9	223	10	264	6	294	14
	4	26	VIIRS	123	10	140	8	157	10	230	10	266	8	301	13
			MODIS	116	9	137	7	160	8	218	11	270	6	298	10
	8	20	VIIRS	126	15	145	14	166	16	232	12	266	11	300	16
			MODIS	113	14	139	13	168	15	225	13	274	10	309	14
Croplands	12	53	VIIRS	137	19	164	15	191	16	234	14	262	14	292	20
			MODIS	139	20	167	16	194	13	232	13	262	15	297	20
	8	11	VIIRS	129	14	148	12	168	13	228	13	264	11	300	15
			MODIS	121	13	144	11	171	12	225	12	275	10	310	14
	4	8	VIIRS	131	11	147	9	164	10	228	11	263	9	298	14
			MODIS	125	10	145	9	168	9	221	10	271	7	300	10
Shrublands/ grasslands	7	33	VIIRS	181	34	199	28	211	42	246	40	273	41	301	43
			MODIS	180	38	202	28	215	41	244	41	269	40	304	38
	10	22	VIIRS	153	57	172	52	146	83	184	82	211	84	240	89
			MODIS	153	57	175	53	152	81	181	80	208	81	244	83
	9	7	VIIRS	131	59	150	56	151	66	199	64	231	63	266	65
			MODIS	126	56	153	56	156	64	191	63	224	62	274	52

differences that were less than one week, with slightly larger differences during green-down (i.e., senescence onset, mid-senescence, and dormancy onset) than during green-up. RMSDs and bias between phenometrics from the MODIS LCD and VIIRS LSP products were consistent across products, and showed no systematic patterns of deviation as a function of location (tile) or land cover type.

Systematic differences between the two products (i.e., bias: VIIRS - MODIS phenometrics) were generally less than one week (absolute bias 4.8 ± 3.0 days; mean ± one standard deviation), and root mean square deviations (RMSDs) were less than two weeks for most phenometrics across land cover classes (10.7 ± 4.3 days) (Table 2). At the same time, modest systematic biases are clearly evident for some phenometrics. For example, mean values for maturity onset from VIIRS were systematically earlier than those from MODIS (−3.6 ± 1.4 days). Similarly, mean senescence onset dates were later for VIIRS than for MODIS (6.6 ± 3.4 days). Moreover, dormancy onset dates from VIIRS were earlier than from MODIS in forest- and cropland-dominated tiles (−4.4 ± 4.3 days). The largest biases were located in woody savannas and were associated with earlier greenup and later dormancy in the MODIS LCD product (12.2 and 8.0 days earlier and 8.3 and 9.0 days later for the forest and croplands tiles, respectively). Semi-arid land cover types (viz., shrublands, grasslands, and savannas) showed modest levels of disagreement across products (i.e., higher RMSDs; 14.7 ± 3.4 days), reflecting higher variation and uncertainty in land surface phenology in semi-arid land cover types that are characterized by low seasonal amplitude in EVI2. Overall, however, agreement was high and bias was low between phenometrics for the two products. In addition, bias and RMSDs between the products across two consecutive years (2013 and 2014) were consistent across land cover types in each of the tiles (Fig. 5).

3.2. Analysis and attribution of differences across products

Comparison of time series derived from VIIRS and MODIS clearly shows that EVI2 time series from each instrument are highly similar, but that MODIS EVI2 time series are smoother and have less high frequency noise relative to VIIRS EVI2 time series. To illustrate, Fig. 6 presents representative EVI2 time series from each sensor for a single pixel from each of six land cover classes. To provide a more comprehensive and quantitative assessment, Table 3 shows results for linear regressions between MODIS and VIIRS EVI2 times series (where MODIS EVI2 is the independent variable in each linear regression), along with the agreement index (AI) for spline and double-logistic model fits to MODIS and VIIRS EVI2 time series (respectively), based on a sample of 10,000 pixels stratified by land cover type from each tile. The estimated regression models have slopes that range from 0.986 to 1.051, intercepts that range from −0.004 to 0.012, and RMSDs range from 0.020 to 0.062, which demonstrate that the EVI2 time series from MODIS and VIIRS are highly comparable with no significant biases. However, estimated AI values for penalized cubic splines fit to MODIS EVI2 time series have slightly higher agreement than double logistic functions fit to VIIRS EVI2 time series, which reflects the greater flexibility of cubic splines relative to logistic functions, in combination with modestly higher noise levels in EVI2 data from VIIRS.

To more fully explore the sources of disagreement between phenometrics from the VIIRS LSP and MODIS LCD products, Fig. 7 shows four scatterplots that attribute observed bias and RMSDs between phenometrics from each product (Table 2) to two key sources: (1) those arising from differences in the input data (i.e., MODIS versus VIIRS); and (2) those arising from differences in the algorithm used to estimate phenometrics (i.e., the MODIS LCD algorithm versus the VIIRS LSP algorithm). To generate these results, we computed phenometrics using the VIIRS LSP algorithm applied to EVI2 time series from both MODIS and VIIRS, and we computed phenometrics from both algorithms using MODIS EVI2 time series (i.e., thereby isolating the magnitude of bias and variance introduced by the algorithm). We used the VIIRS LSP algorithm in the former case because the VIIRS LSP product is designed to replace the MODIS LCD product, and we used MODIS data in the latter case because MODIS EVI2 data are less noisy than VIIRS EVI2 data. In Fig. 7, the vertical axes correspond to the biases (Fig. 7a and c) and RMSDs (Fig. 7b and d) between the MODIS LCD and VIIRS LSP products from Table 2. In Fig. 7a and b, the horizontal axes correspond to biases

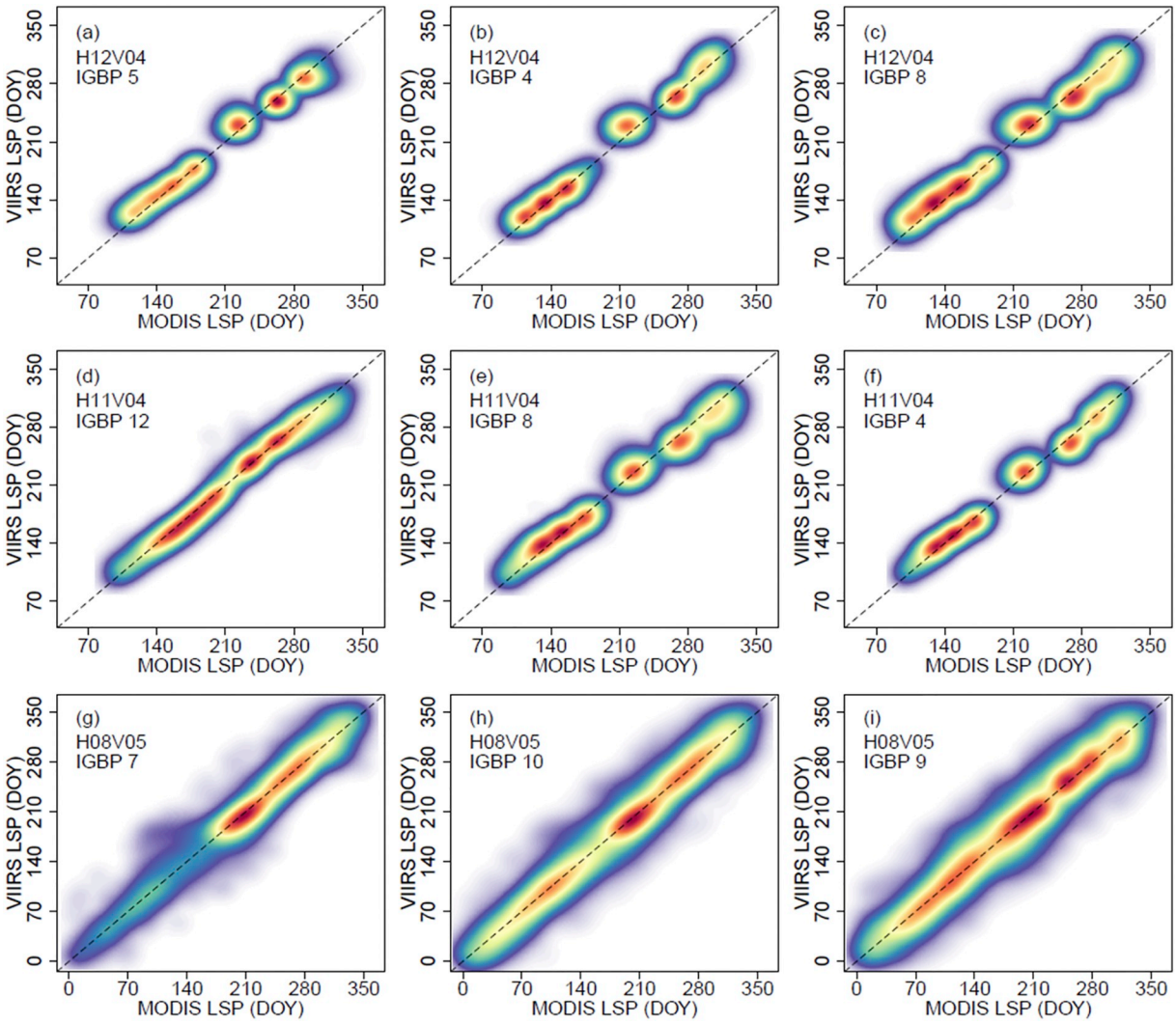

Fig. 4. Comparison of phenometrics from the VIIRS LSP and the MODIS LCD products in 2013, stratified by the three most common land cover types in each tile. Red indicates high density and light purple indicates low density of observations. The dashed lines show 1:1 agreement. See caption of Table 1 for IGBP class names and statistical summaries for each phenometric. (For interpretation of the references to colour in this figure legend, the reader is referred to the web version of this article.)

and RMSDs computed using phenometrics estimated using the VIIRS LSP algorithm applied to both VIIRS and MODIS EVI2 data (isolating the effect of input data). In Fig. 7c and d, on the other hand, the horizontal axes correspond to differences computed using phenometrics derived from the VIIRS LSP and MODIS LCD algorithms applied to MODIS EVI2 data (isolating the effect of the algorithms).

The results shown in Fig. 7a demonstrate that bias in phenometrics between the two products (i.e., bias in the product-to-product comparison) are uncorrelated with bias induced from input data, and that the magnitude of bias derived from input data is much smaller than the magnitude of bias between the two products. Fig. 7c, however, shows that biases induced by algorithm differences have the same magnitude and are correlated with the biases found in the product-to-product comparison. These results imply that the majority of systematic bias between the two products can be attributed to differences in the algorithms, not the input data (see also, Figs. A1 and A2 in the Appendix). Fig. 7b and d, on the other hand, show that RMSDs are correlated and have similar magnitude, and so differences in input data and algorithms contribute equally to non-systematic differences (i.e., random errors) between the products.

To further quantify how noise in input data affects errors in estimated phenometrics, Fig. 8 shows results from the statistical simulation described in Section 2.3, where the vertical axes in Fig. 8a and b correspond to the RMSD values from the two products in Table 2, and the horizontal axes correspond to the RMSDs in phenometric retrievals induced by the inherent uncertainties in both VIIRS and MODIS NBAR data across land cover types within each tile. These results show that despite high agreement between NBAR EVI2 time series from MODIS and VIIRS, and excellent model fits to time series, errors arising from noise in EVI2 time series can introduce considerable uncertainty into the phenometrics. More specifically, when noise levels in input data are low, differences in phenometrics are mostly due to algorithmic uncertainty; as noise levels increase, errors in phenometrics are mostly caused by noise in the input data. Overall, errors from phenometrics estimated using MODIS NBAR data are marginally (but consistently) lower than those from VIIRS NBAR data (7.3 versus 8.7 days on overall

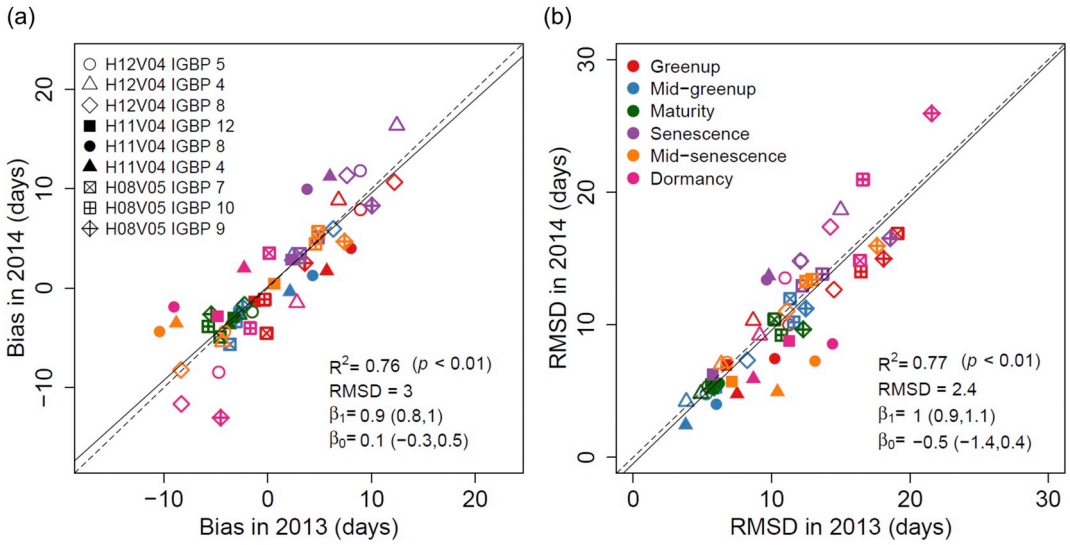

Fig. 5. Comparison of (a) bias and (b) RMSD between phenometrics from the VIIRS LSP and MODIS LCD products from consecutive two years (2013 and 2014). Bias is calculated as VIIRS – MODIS; RMSD is the root mean squared deviation. Different symbols denote different land cover types in different tiles, and different colors denote different phenometrics. Values in parentheses indicate ± 1 standard deviation. The solid and dashed lines are regression fits and 1:1 lines, respectively. See caption of Table 1 for IGBP class names.

means, respectively), and these errors are strongly correlated ($R^2 = 0.98$, $p < 0.001$; Fig. 8c).

3.3. Comparison with Landsat phenology

Fig. 9 presents a comparison between phenometrics derived from Landsat with corresponding dates derived from the VIIRS LSP and MODIS LCD products. It shows that results from all three instruments were in close agreement across all 22 sidelaps examined in this study. For SOS, both products showed strong agreement with results from Landsat ($R^2 = 0.94$ and 0.95 for VIIRS and MODIS, respectively), with VIIRS results tending to be biased later relative to Landsat for earlier greenup dates, and biased earlier for later dates (95% confidence interval for the slope of the regression = 1.2 ± 0.10). RMSD values were less than five days for both VIIRS and MODIS SOS dates relative to Landsat. For EOS, both products again showed good agreement, but not quite as strong as those observed for SOS. EOS from MODIS exhibited better agreement with Landsat than EOS from VIIRS ($R^2 = 0.57$ and 0.82 for VIIRS and MODIS, respectively). Further, EOS dates from VIIRS were biased early relative to those from Landsat. Nevertheless, overall RMSD values were less than one week for both products. At regional scale (i.e., aggregated to EPA level II ecoregions), both products showed good agreement with Landsat. For SOS, RMSDs across six different ecoregions ranged from 2.8 to 13.2 with a mean of 7.1 for VIIRS, and from 3.0 to 16.4 with a mean of 6.8 for MODIS (Table 4). For EOS, RMSDs ranged from 4.2 to 14.9 with a mean of 8.5 for VIIRS and from 3.3 to 10.9 with a mean of 6.4 for MODIS (Table 5).

3.4. Comparison with PhenoCam phenology

Phenometrics derived from VIIRS and MODIS showed generally strong agreement with phenometrics estimated from PhenoCam imagery, but with more scatter relative to dates estimated from Landsat (Fig. 10). Disagreement was highest for evergreen needleleaf sites, where phenological amplitude is low and difficult to detect using vegetation indices such as the G_{CC} and EVI2. Thus, we do not expect

Table 2
Statistical agreement between the VIIRS LSP and MODIS LCD products in 2013. IGBP denotes land cover type. Bias is calculated as VIIRS – MODIS; RMSD is the root mean squared deviation. See caption of Table 1 for IGBP class names.

Tile ID	IGBP	Greenup onset		Date at mid-greenup		Maturity onset		Senescence onset		Date at mid-senescence		Dormancy onset	
		Bias	RMSD	Bias	RMSD	Bias	RMSD	Bias	RMSD	Bias	RMSD	Bias	RMSD
Forests	5	8.9	11.2	3.1	5.3	−1.5	5.4	8.9	12.1	−4.1	6.8	−4.7	11.0
	4	6.8	8.7	2.4	3.8	−2.7	4.9	12.4	15.0	−4.3	6.4	2.8	9.1
	8	12.2	14.5	6.3	8.2	−2.2	5.8	7.6	12.1	−8.3	11.1	−8.3	14.2
Croplands	12	−1.3	6.7	−2.8	6.0	−3.3	5.6	2.3	5.8	0.6	7.1	−4.8	11.3
	8	8.0	10.2	4.4	6.0	−3.1	6.2	3.8	9.6	−10.4	13.1	−9.0	14.4
	4	5.7	7.5	2.2	3.8	−3.7	5.7	6.0	9.8	−8.8	10.4	−2.3	8.7
Shrublands/grasslands	7	−0.1	19.1	−3.6	11.3	−4.6	10.2	3.1	12.2	4.9	12.5	0.2	16.4
	10	−0.3	16.5	−3.1	11.6	−5.7	10.7	4.9	13.7	4.6	12.9	−1.7	16.6
	9	3.6	18.1	−2.4	12.5	−5.4	12.3	10.1	18.6	7.4	17.6	−4.5	21.6

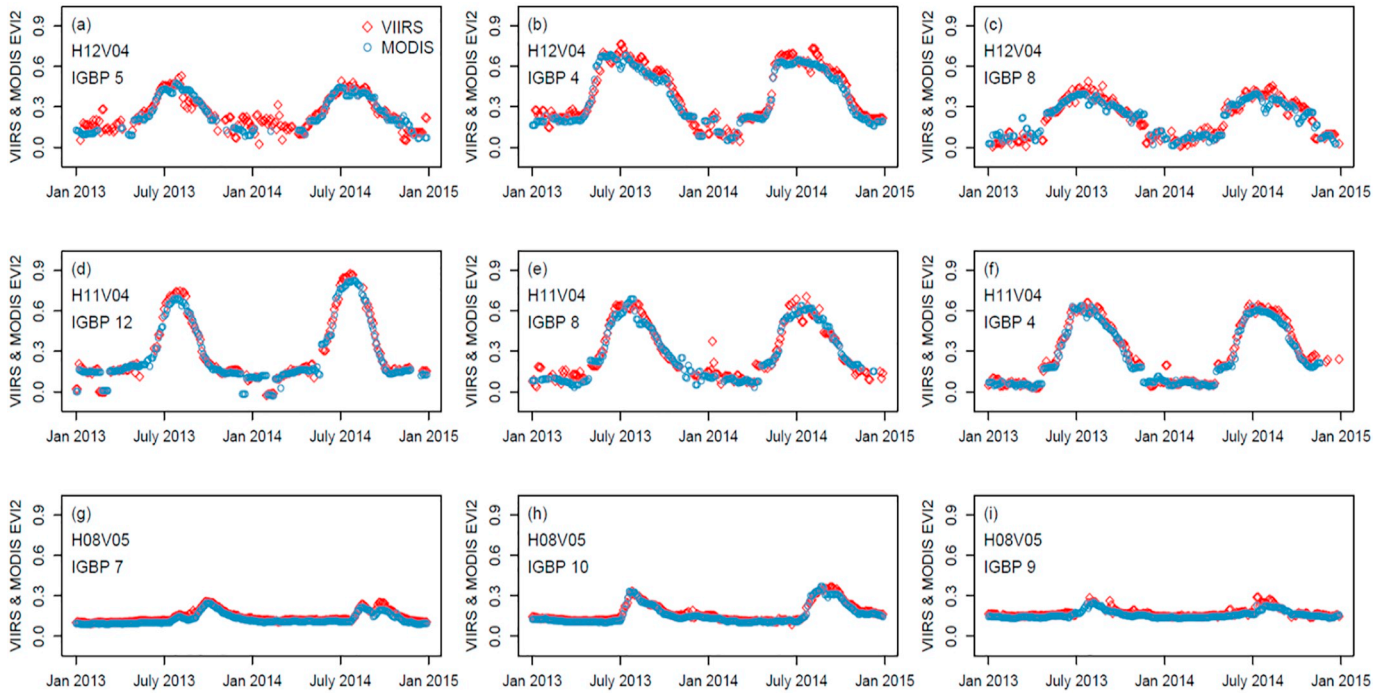

Fig. 6. NBAR EVI2 time series from VIIRS (diamonds) and MODIS (circles), stratified by the three most common land cover types in each tile during 2013 and 2014. Each dot represents 3-day composites NBAR EVI2 value from each instrument. See caption of Table 1 for IGBP class names.

strong correspondence between ground-based and satellite-derived retrievals in these systems. Other land cover types (e.g., deciduous broadleaf forests and croplands), on the other hand, showed agreement that was comparable to those obtained with Landsat-derived SOS and EOS dates (Table 6).

It is important to understand that PhenoCam and coarse spatial resolution sensors, such as VIIRS and MODIS, observe the surface with very different fields of view. Hence, comparison of VIIRS LSP and MODIS LCD products with PhenoCam results depends heavily on the representativeness of the region of interest in PhenoCam imagery used to generate G_{CC} time series relative to the field of view captured by 500 m MODIS and VIIRS pixels. Fig. 11 illustrates this issue at the Jasper Ridge PhenoCam

Table 3
Linear regression and AI statistics for EVI2 time series from VIIRS and MODIS, stratified by the three most common land cover types in each tile. See caption of Table 1 for IGBP class names. RMSD is the root mean squared deviation; 25%, 50%, 75% represent the 1st quartile, median, and 3rd quartile, respectively.

Tile ID	IGBP	Linear regression				Agreement index				
		Slope	Intercept	R^2	RMSD	Product	Mean	25%	50%	75%
Forests	5	0.986	0.007	0.809	0.058	VIIRS	95.6	94.6	96.9	98.1
						MODIS	98.7	98.5	99.0	99.3
	4	1.016	0.012	0.880	0.062	VIIRS	97.9	97.5	98.4	98.9
						MODIS	99.0	98.8	99.1	99.4
	8	1.051	−0.004	0.889	0.057	VIIRS	96.7	96.0	97.6	98.4
						MODIS	98.8	98.7	99.2	99.4
Croplands	12	1.015	0.002	0.960	0.043	VIIRS	98.3	98.0	98.6	99.1
						MODIS	99.4	99.3	99.5	99.7
	8	1.024	−0.002	0.933	0.046	VIIRS	97.9	98.0	98.9	99.3
						MODIS	99.3	99.3	99.5	99.6
	4	1.014	0.002	0.942	0.044	VIIRS	98.8	98.8	99.2	99.4
						MODIS	99.5	99.4	99.5	99.6
Shrublands/grasslands	7	1.018	0.011	0.913	0.020	VIIRS	86.9	84.4	93.0	96.9
						MODIS	95.2	94.4	97.3	98.5
	10	1.018	0.009	0.934	0.023	VIIRS	91.5	90.5	96.6	98.5
						MODIS	96.6	96.5	98.5	99.4
	9	1.016	0.008	0.899	0.024	VIIRS	89.8	87.1	94.4	97.7
						MODIS	96.5	95.7	98.2	99.3

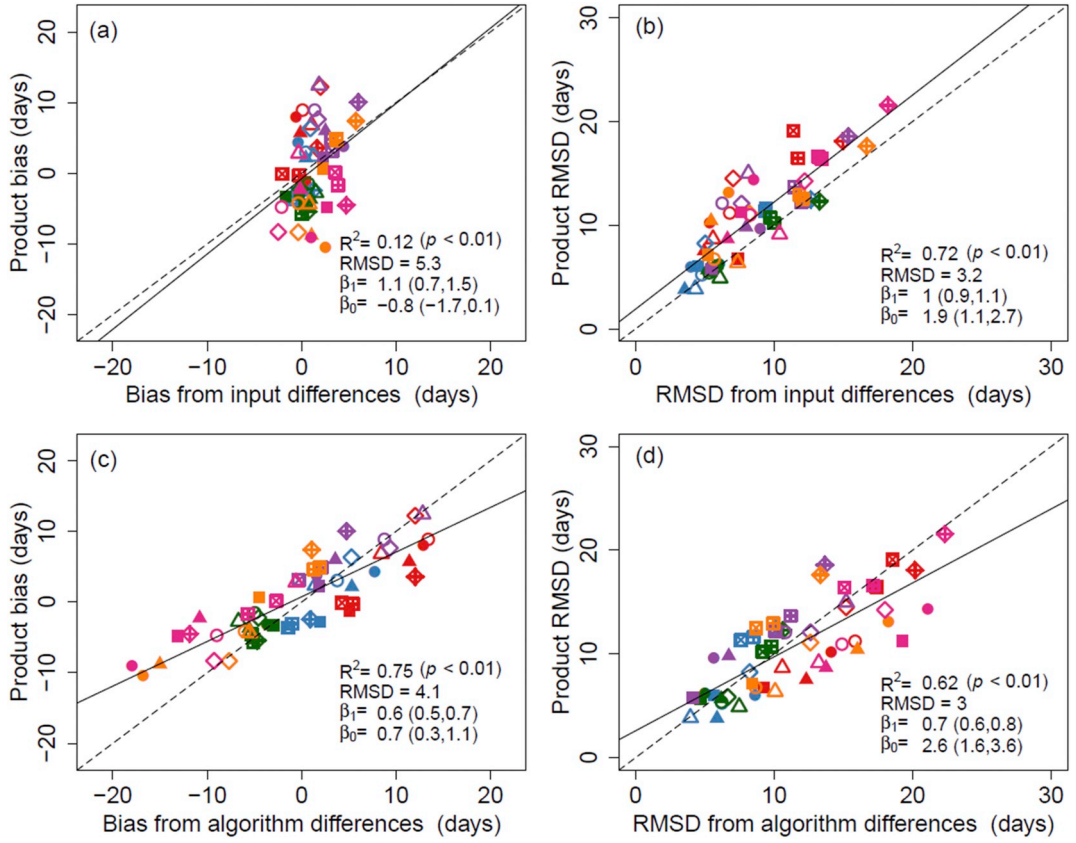

Fig. 7. Differences in phenometrics from MODIS LCD versus VIIRS LSP derived from differences in input (EVI2 time series) versus algorithms. Panels (a) and (b) illustrate differences in phenometrics arising from different input data, while panels (c) and (d) illustrate differences in phenometrics arising from the different algorithms. Bias represents differences in phenometrics; RMSD is the root mean squared deviation. Values in parentheses indicate ± 1 standard deviation. The solid and dashed lines are the regression and 1:1 lines, respectively. Different shapes denote different land cover types in different tiles and different colors denote different phenometrics. See Fig. 5 for symbols and colors legends.

site, which provides a good illustration of this challenge. Specifically, Fig. 11a shows the 500 m MODIS and VIIRS pixel overlain on 30 m Landsat imagery centered over the Jasper Ridge PhenoCam site, and Fig. 11b shows the region of interest used to generate G_{CC} time series from PhenoCam imagery. As these two panels show, a large portion of the land cover located within the 500 m pixel consists of tree cover. The PhenoCam

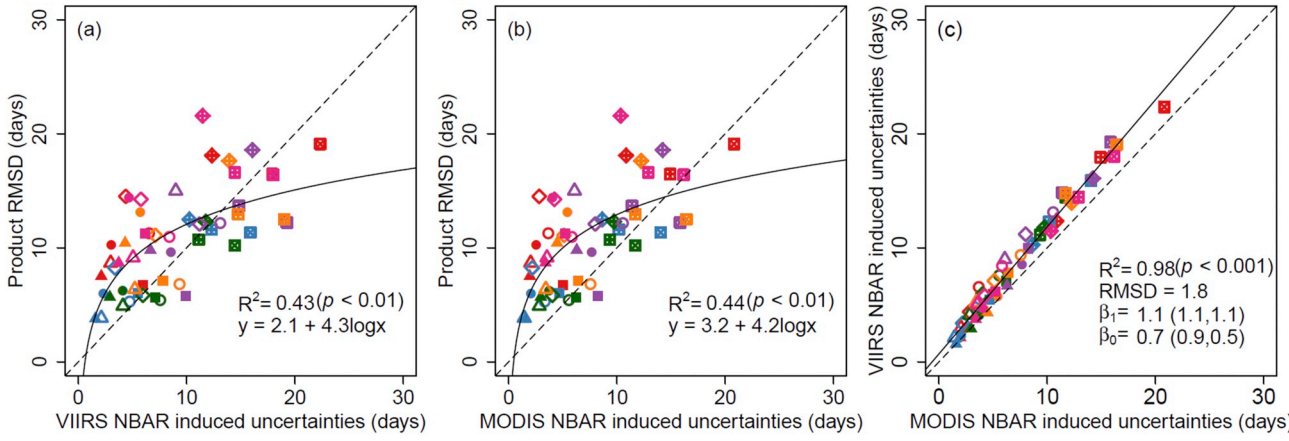

Fig. 8. Analysis of errors in phenometrics between the VIIRS LSP and MODIS LCD products versus errors introduced by uncertainties in input data. Panels (a) and (b) illustrate errors in phenometrics between the two products versus errors arising from uncertainties in VIIRS and MODIS input data, respectively; panel (c) illustrates relationship between errors arising from uncertainties in VIIRS and MODIS input data. Values in parentheses in panel (c) indicate ± 1 standard deviation. The solid and dashed lines are the regression and 1:1 lines, respectively. Different shapes denote different land cover types in different tiles and different colors denote different phenometrics. See Fig. 5 for symbols and colors legends.

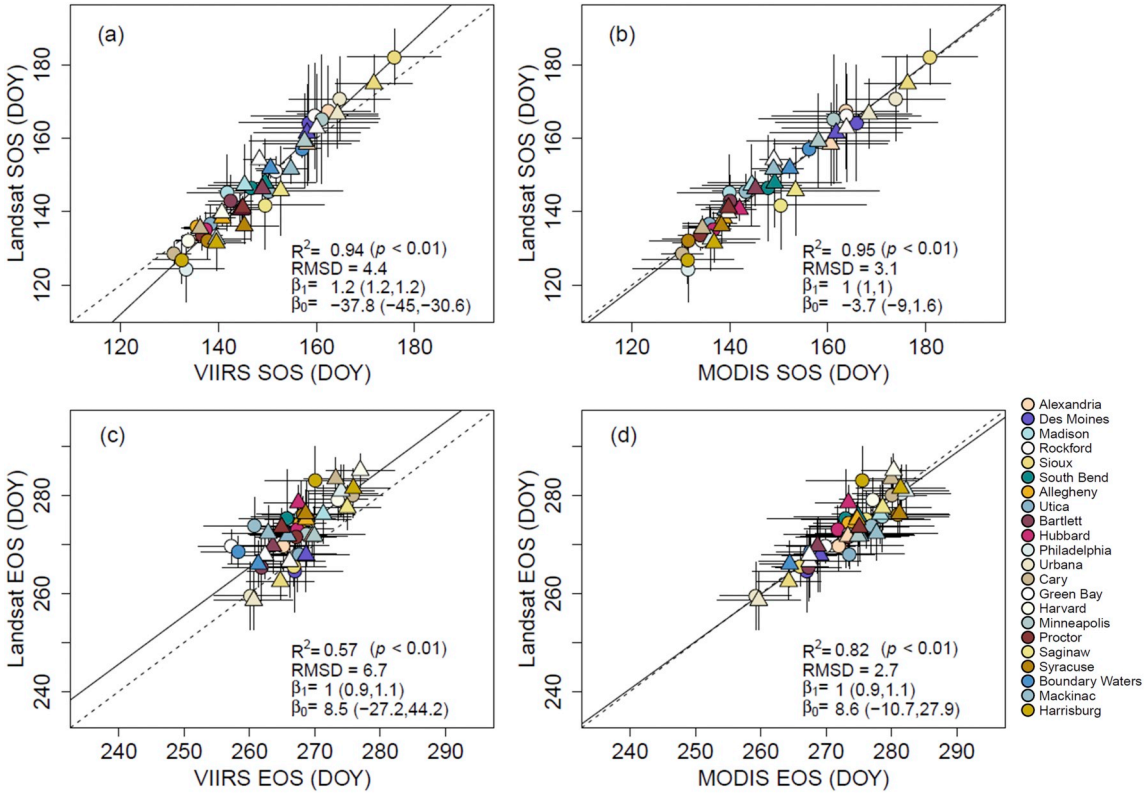

Fig. 9. Comparison of the VIIRS LSP and MODIS LCD products with phenometrics derived from Landsat in 2013 and 2014. Different colors denote different Landsat sidelaps and different shapes denote different years (circles: 2013; triangles: 2014). Values in parentheses indicate ± 1 standard deviation. The solid and dashed lines are the regression and 1:1 lines, respectively. See Tables 4 and 5 for statistical summaries for each product in each sidelap.

Table 4
Statistical agreement of the VIIRS LSP and MODIS LCD products with SOS transition dates derived from Landsat in 2013. Bias is calculated as VIIRS – Landsat and MODIS – Landsat; RMSD is the root mean squared deviation; $\bar{x}$ is the mean and σ is one standard deviation. Ecoregions are the EPA level 2 ecoregions: AH: Atlantic Highlands; CUP: Central USA Plains; MWP: Mixed Woods Plains; MWS: Mixed Woods Shield; OA: Ozark/Ouachita-Appalachian Forests; TP: Temperate Prairies.

Spring												
Site name	Ecoregion	Latitude/longitude	Landsat		VIIRS				MODIS			
			$\bar{x}$	σ	$\bar{x}$	σ	Bias	RMSD	$\bar{x}$	σ	Bias	RMSD
Bartlett	AH	44.62/–71.19	143	6.9	142	4.6	−0.5	5.8	140	4.0	−2.9	7.0
Hubbard	AH	43.90/–71.40	135	4.6	137	4.4	2.1	4.6	137	3.6	1.4	4.0
Philadelphia	AH	40.52/–75.63	124	9.1	133	7.8	9.0	11.5	131	11.3	7.1	11.5
Utica	AH	43.19/–74.73	137	5.1	138	3.8	1.6	4.2	136	5.5	−0.9	4.4
Rockford	CUP	41.76/–89.11	166	14.4	160	13	−6.5	8.9	164	15.2	−2.3	6.4
Urbana	CUP	40.51/–87.99	171	11.5	165	10.3	−5.9	9.5	174	10.1	3.2	7.3
Alexandria	MWP	46.03/– 95.34	167	12.4	162	8.6	−5.0	9.6	164	10.8	−3.7	8.4
Allegheny	MWP	41.76/–78.29	136	2.5	136	2.6	−0.3	2.9	135	3.5	−0.8	3.0
Cary	MWP	41.77/–73.66	129	3.1	131	3.6	2.3	3.5	130	4.3	1.8	3.6
Green Bay	MWP	46.04/–89.16	151	4.0	152	3.9	0.6	4.1	149	3.1	−1.8	4.2
Harvard	MWP	42.47/–71.89	132	2.2	134	2.5	1.6	2.8	134	2.6	2.1	3.1
Madison	MWP	43.19/–90.18	145	10.3	142	8.1	−3.4	7.4	140	10.6	−5.2	8.2
Minneapolis	MWP	44.61/–92.77	165	17.5	161	11.8	−4.1	10.9	161	15.3	−4.0	9.9
Proctor	MWP	44.62/–72.68	134	4.1	137	4.1	3.1	4.6	134	4.5	0.4	4.2
Saginaw	MWP	43.19/–84.00	142	11.9	150	12.1	7.8	13.2	150	17.4	8.7	16.4
South bend	MWP	41.76/–86.02	146	14.3	147	11	0.3	8.3	148	15.8	1.4	8.2
Syracuse	MWP	43.19/–76.27	132	5.0	138	6.7	5.8	9.0	132	7.9	−0.5	7.2
Boundary waters	MWS	47.46/–91.71	157	2.5	157	3.7	−0.1	3.4	156	3.5	−0.9	3.6
Mackinac	MWS	46.04/–84.53	146	4.5	150	5.5	4.7	5.9	143	5.8	−2.3	4.4
Harrisburg	OA	40.52/–77.17	127	6.4	132	5.9	5.6	8.9	131	9.3	4.5	10.3
Des Moines	TP	41.76/– 92.20	164	15.8	158	14.2	−5.8	9.4	166	16.6	1.7	8.0
Sioux	TP	43.19/–94.78	182	7.5	176	9.6	−6.2	8.3	181	9.7	−1.3	5.2
Average	–	–	147	8.0	147	7.2	0.3	7.1	147	8.7	0.3	6.8

Table 5
Statistical agreement between the VIIRS LSP and MODIS LCD products with EOS transition dates derived from Landsat in 2013. Bias is calculated as VIIRS – Landsat and MODIS – Landsat; RMSD is the root mean squared deviation; $\bar{x}$ is the mean and σ is one standard deviation. See Table 4 for the ecoregions.

Autumn											
Site name	Ecoregion	Landsat		VIIRS				MODIS			
		$\bar{x}$	σ	$\bar{x}$	σ	Bias	RMSD	$\bar{x}$	σ	Bias	RMSD
Bartlett	AH	265	6.8	262	6.1	−3.4	6.1	267	5.0	2.0	5.7
Hubbard	AH	273	4.7	267	5.6	−5.8	7.4	272	5.1	−1.3	3.3
Philadelphia	AH	280	5.8	274	5.3	−6.1	8.5	282	7.5	1.1	7.1
Utica	AH	268	3.0	268	5.6	−0.4	4.8	274	8.4	5.5	9.5
Rockford	CUP	268	7.6	267	6.5	−0.5	5.0	269	8.7	0.8	4.5
Urbana	CUP	259	6.8	260	5.6	0.6	4.4	259	5.5	−0.3	4.1
Alexandria	MWP	270	5.1	265	6.9	−4.6	8.2	272	9.9	2.2	8.1
Allegheny	MWP	274	3.0	268	4.0	−6.6	7.6	273	5.3	−0.9	5.2
Cary	MWP	280	4.7	276	4.6	−4.3	6.1	280	5.3	0.0	5.3
Green Bay	MWP	270	3.5	257	5.0	−12.4	13.6	270	4.5	0.2	4.3
Harvard	MWP	279	4.3	273	4.5	−5.7	6.7	277	5.1	−2.0	3.5
Madison	MWP	276	7.2	268	7.6	−7.8	11.2	279	10.1	2.9	9.0
Minneapolis	MWP	272	6.4	269	8.9	−3.4	9.3	273	9.9	1.3	7.9
Proctor	MWP	271	3.6	267	6.2	−4.4	6.7	273	8.0	2.0	7.3
Saginaw	MWP	275	5.9	269	6.6	−6.2	9.2	276	9.9	1.0	8.2
South Bend	MWP	275	10.0	266	7.4	−9.6	12.4	273	12.0	−2.3	7.4
Syracuse	MWP	276	3.8	268	6.3	−7.9	9.6	281	7.9	4.9	8.2
Boundary waters	MWS	268	3.1	258	5.7	−10.2	11.6	268	5.2	−0.9	4.7
Mackinac	MWS	274	5.9	261	7.7	−13.0	14.9	277	9.5	3.2	8.0
Harrisburg	OA	283	7.0	270	7.7	−13.0	14.6	276	8.5	−7.6	10.9
Des Moines	TP	264	8.3	267	7.3	2.5	5.4	267	8.3	2.5	4.9
Sioux	TP	266	4.1	267	4.9	1.2	4.2	266	4.4	0.5	3.6
Average	–	272	5.5	267	6.2	−5.5	8.5	273	7.5	0.7	6.4

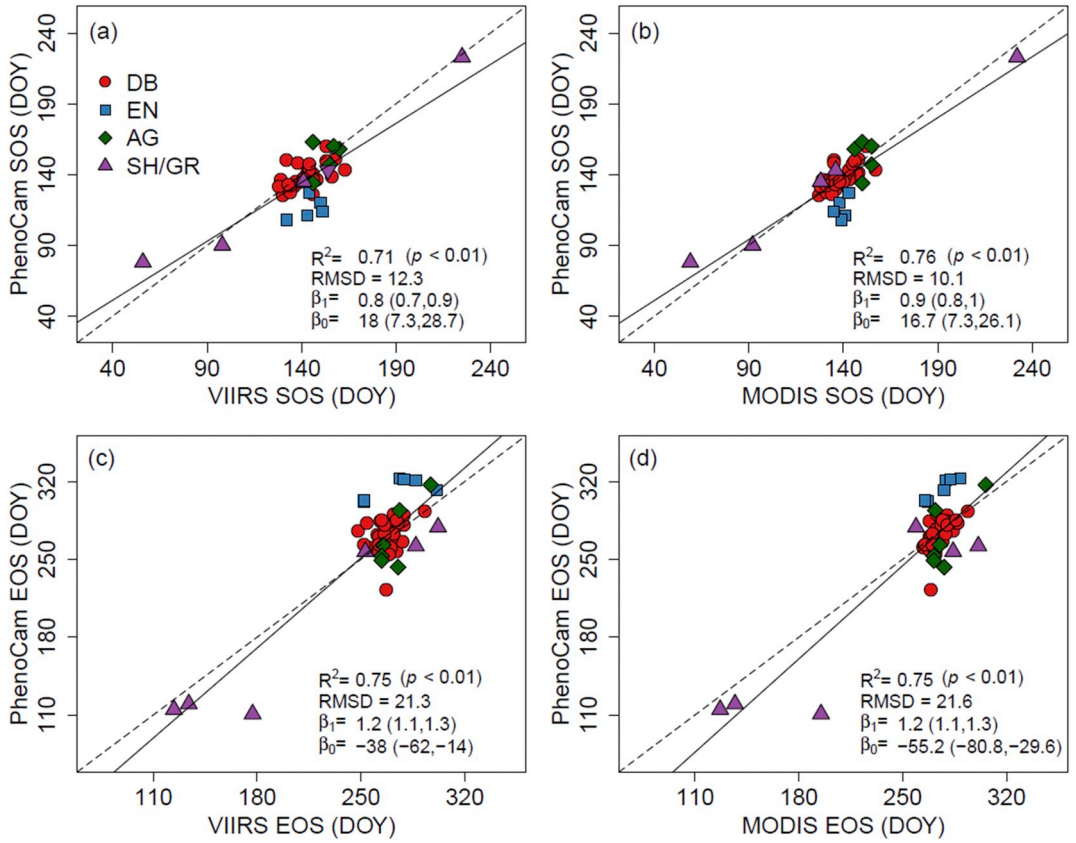

Fig. 10. Comparison of the VIIRS LSP and MODIS LCD products with phenometrics derived from PhenoCam imagery in 2013 and 2014. SOS and EOS represent the DOY at mid-greenup and mid-down for the VIIRS and MODIS products, respectively. Different colors denote different vegetation types (see panel a) at each PhenoCam site (DB: deciduous broadleaf; EN: evergreen needleleaf; AG: agricultural; GR: grassland; SH: shrubland). Values in parentheses indicate ± 1 standard deviation. The solid and dashed lines are the regression and 1:1 lines, respectively. See Table 6 for the statistical agreement between PhenoCam and both VIIRS and MODIS SOS and EOS dates, for each vegetation type.

Table 6
Statistical agreement between the VIIRS LSP and MODIS LCD products with phenometrics derived from PhenoCam imagery. n is the number of site-years; bias is calculated as VIIRS – PhenoCam and MODIS – PhenoCam; RMSD is the root mean squared deviation. See Fig. 10 for the vegetation type.

Vegetation type	n	PhenoCam		VIIRS				MODIS			
		$\bar{x}$	σ	$\bar{x}$	σ	Bias	RMSD	$\bar{x}$	σ	Bias	RMSD
Spring											
DB	38	137	7.7	141	8.3	4.2	8.3	138	7.1	1.4	5.8
EN	5	116	7.6	144	7.6	28.0	28.8	139	3.0	23.2	24.0
AG	5	152	11.9	153	6.5	0.4	10.1	151	3.8	−1.2	11.5
GR/SH	5	134	57.2	135	63.5	1.0	11.9	129	65.1	−4.4	10.4
Autumn											
DB	38	271	13.7	268	8.3	−2.9	13.7	274	6.7	3.1	11.2
EN	6	314	9.6	275	19.5	−39.3	41.7	277	9.1	−37.2	37.3
AG	6	270	29.3	274	12.8	3.7	18.7	279	13.6	9.0	21.5
GR/SH	6	191	82.9	213	78.0	22.2	31.1	217	75.2	26.5	41.1

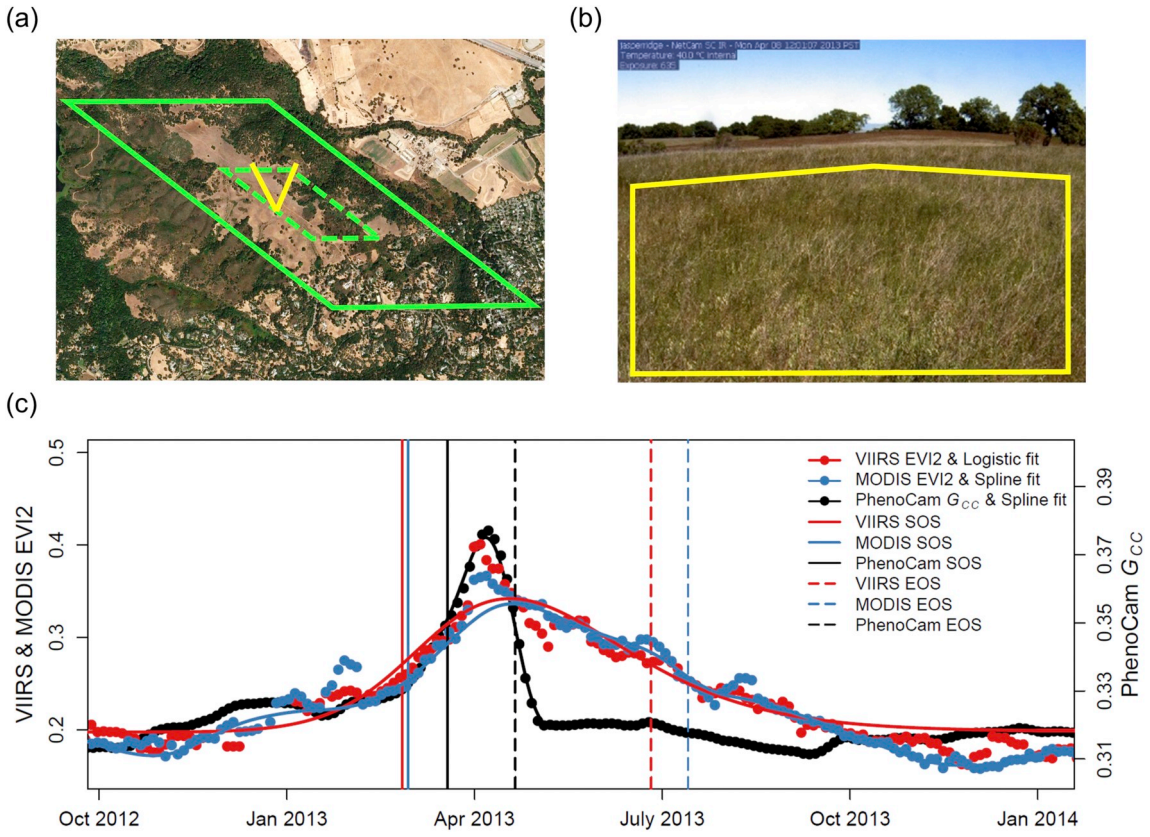

Fig. 11. VIIRS and MODIS pixels over the Jasper Ridge PhenoCam site (a), a PhenoCam image and region of interest used to generate G_{CC} time series (b), and time series of EVI2 from VIIRS, and MODIS, along with G_{CC} from PhenoCam (c). Phenometrics from each time series are shown as vertical lines. In panel (a), the solid and dashed green lines represent a 3 by 3 window and the 500 m pixel centered at the camera's location, respectively; the yellow lines indicate the field of view of the PhenoCam. In panel (b), the yellow box represents the extracted region of interest from PhenoCam imagery. (For interpretation of the references to colour in this figure legend, the reader is referred to the web version of this article.)

region of interest (Fig. 11b), however, includes only herbaceous vegetation. As a result, the PhenoCam G_{CC} time series (Fig. 11c) captures the phenology of grasses at the site, which is different from the phenology measured in EVI2 time series from VIIRS and MODIS that includes substantial contributions from over-story tree phenology. This target mismatch leads to clear differences in observed phenology, especially during the green-down phase.

4. Discussion

The land product suite from MODIS provides an 18-year (and growing) record of global land properties and processes during an era when global environmental change has been accelerating. Originally designed as a research mission, MODIS has evolved to provide a critical source of time series observations supporting operational

environmental monitoring and global change science. With the MODIS era approaching its end, the VIIRS instrument has been designated to provide continuity with measurements and products from MODIS. In this paper, we evaluated the suitability of the VIIRS Land Surface Phenology product for providing long-term continuity with the MODIS Land Cover Dynamics product, focusing on two main elements. First, we performed an extensive comparison of the MODIS LCD and VIIRS LSP products, focusing on the nature, magnitude, and sources of differences between the products. Second, we compared both products against two independent sources of land surface phenology data.

4.1. Comparison of MODIS LCD and VIIRS LSP products

Our results indicate that the MODIS LCD and VIIRS LSP products are qualitatively and quantitatively similar, but also identify subtle differences arising from three key sources:

(i) *Instrument differences*. Although VIIRS was originally conceived to provide observation continuity with MODIS (Justice et al., 2013), the properties of these two sensors are different, which results in modest discrepancies between operational products from each instrument. Most importantly in the context of this work, both the VIIRS LSP and MODIS LCD products use NBAR surface reflectance as their primary input. Our analysis identified modest differences in NBAR EVI2 time series from VIIRS versus MODIS that propagate into the VIIRS LSP and MODIS LCD products (Figs. 7 and 8). Consistent with Liu et al. (2017), who reported that the VIIRS NBAR product is comparable with the MODIS NBAR product, our results suggest that NBAR EVI2 time series from each sensor are in good agreement and do not show systematic differences or biases (Fig. 6 and Table 3). However, similar to Zhang et al. (2017a), AI values computed from VIIRS and MODIS NBAR EVI2 time series indicate that EVI2 time series from MODIS are more stable than those from VIIRS. In addition, errors in phenometrics induced by uncertainty in VIIRS NBAR data were larger than those induced by uncertainty in MODIS NBAR data (Fig. 8). While we are not able to conclusively attribute this difference to a specific source, the most likely explanation for observed differences in EVI2 time series is lower data density available from VIIRS relative to MODIS. Specifically, NBAR data from VIIRS are based on a single (1:30 pm equatorial) overpass, whereas MODIS NBAR data are computed using observations from both the morning (10:30 am equatorial) MODIS-Terra and afternoon (1,30 pm equatorial) MODIS-Aqua overpasses (Zhang et al., 2017a).

(ii) *Differences in NBAR EVI2 pre-processing*. Both algorithms depend on successful retrieval of a “background” or seasonal minimum EVI2 value at each pixel. The VIIRS LSP algorithm uses land surface temperature in addition to snow flags from the VIIRS NBAR product to identify and remove snow-contaminated pixels, while the MODIS LCD algorithm only uses snow flags from the MODIS NBAR product in combination with NDSI values. These approaches reflect modestly different assumptions regarding the quality of NBAR snow flags, and have the potential to induce subtle differences between the two products. In particular, the MODIS LCD product tends to have slightly longer growing season lengths than corresponding values from the VIIRS LSP product in temperate regions (e.g., forests and croplands tiles, Table 2 and Fig. 4). This effect appears to be limited to temperate regions, and we did not find other examples or evidence of significant and systematic differences between phenometrics from each product. In addition, disagreement between VIIRS LSP and MODIS LCD phenometrics was more prevalent in semi-arid land cover types (i.e., higher RMSDs for shrublands and grasslands in Table 2). This issue is not unexpected because low seasonal amplitude in the EVI2 time series (as shown in Fig. 6) tends to increase uncertainty in estimated LSP metrics (Fig. 8), and because subtle differences in smoothing and gap filling will lead to differences in estimated phenometrics (Fig. 7).

(iii) *Differences in the method used for EVI2 time series modeling*. Currently, there is no consensus in the land surface phenology community regarding optimal methods and algorithms for deriving land surface phenology metrics. The algorithm used to generate the VIIRS LSP product uses a logistic model to provide a simple, bounded, and continuous function for modeling EVI2 variation associated with leaf emergence, maturation, and senescence (Zhang, 2015). This approach is widely used for modeling phenological dynamics in biological systems, and provides a framework that is widely accepted and interpretable. The Collection 6 MODIS LCD product, on the other hand, uses penalized cubic splines to model temporal variation in NBAR EVI2 time series (Gray et al., 2019). Unlike logistic models, local fitting techniques such as splines are more flexible and are therefore able to capture a broader range of temporal dynamics (e.g., asymmetric phenology; Verma et al., 2016). At the same time, because penalized cubic splines provide local fits to data, they are more sensitive to gaps and high frequency variation in EVI2 time series. Hence, in situations where missing data are pervasive, penalized cubic splines are less robust than logistic models (Zhang et al., 2018b). Further, the different methods for selecting transition dates in each algorithm (i.e., the curvature change rate versus amplitude threshold) can introduce differences between the two products, and Klosterman et al. (2014) report that landscape heterogeneity can introduce uncertainty in curve fit estimates during green-down. Consistent with these results, our analyses show that differences between MODIS LCD and VIIRS LSP results in mixed forests are marginally larger than those found in deciduous broadleaf forests during the green-down phase, especially for senescence onset (IGBP 5 versus 4; Table 2), and we find larger differences in EOS than in SOS (e.g., Fig. 11).

4.2. Comparisons with independent data

In addition to comparing results from each algorithm and product, we also assessed agreement of each product with LSP measurements from Landsat and PhenoCam data. Results from Landsat have the advantage of being estimated from remote sensing using instrumentation with similar spectral properties to MODIS and VIIRS, but at finer spatial resolution. The PhenoCam Dataset V1.0 (Richardson et al., 2018a) based on digital repeat photography, on the other hand, provides a source of “near-surface” remote sensing that covers a wide range of biomes. Results from these comparisons show that the VIIRS LSP and MODIS LCD products both agree well with phenometrics derived from Landsat (Fig. 9). Across six ecoregions spanning the Central and Northeastern U.S, the mean RMSD for SOS was roughly one week for both products (Table 4). RMSDs between Landsat EOS and corresponding metrics from MODIS and VIIRS were modestly higher, but were also on the order of one week (Table 5). Interestingly, even though agreement with Landsat SOS was lower at local scale for both the MODIS LCD and VIIRS LSP products, overall mean RMSD at the scale of ecosystems was comparable across instruments, which suggests that even though local uncertainty in SOS retrievals is significant, they do not appear to be biased. EOS values for the MODIS LCD product show

modestly higher agreement with Landsat EOS dates relative to VIIRS LSP values. However, closer inspection indicates that overall bias for both products is similar and quite low, which implies that such differences may be explained by the fact that the LPA uses cubic splines to fit EVI time series from Landsat (i.e., similar to the MODIS LCD product), while the VIIRS LSP does not.

Evaluation of satellite-derived land surface phenology products with PhenoCam-derived phenometrics is challenging, and lower agreement between phenometrics from PhenoCam and both the MODIS LCD and VIIRS LSP products can be explained by two main factors. First, because PhenoCams do not generally provide imagery acquired in near infrared wavelengths (Yang et al., 2014), phenometrics from PhenoCam are estimated using a vegetation index based on visible bands (i.e., G_{CC}, Sonnentag et al., 2012). Richardson et al. (2018b) performed a comprehensive assessment of G_{CC} time series and phenometrics derived from PhenoCam against both MODIS NDVI and LCD data using the PhenoCam Dataset V1.0, and showed good agreement in both cases. However, similar to our results, they identified differences in the sensor field of view, in combination with landscape heterogeneity, as key sources of disagreement. Consistent with Richardson et al. (2018b), our results show that, with the exception of evergreen needleleaf sites, phenometrics derived from PhenoCam G_{CC} time series agree reasonably well with the VIIRS LSP and MODIS LCD products, but that sub-pixel heterogeneity within satellite-based remote sensing pixels can cause substantial discrepancies in estimated phenometrics (Fig. 11).

5. Conclusion

Phenology is a fundamental regulator of many ecological processes, is readily observable and easily understood by the public, and is widely viewed to be an important diagnostic of ecosystem response to climate change. Thus, high-quality long-term records related to phenology, including those derived from satellite remote sensing, are essential. In this paper, we evaluated and quantified similarities and differences between two operational LSP products. Our specific motivation for this work was to address the question of whether the VIIRS LSP product provides continuity with the MODIS LCD product for long-term studies of land surface phenology. As part of our analysis, we compared EVI2 time series from each instrument, quantified random and systematic differences between phenometrics from each sensor, and conducted a multi-scale comparison of the VIIRS LSP and MODIS LCD products with phenometrics derived from Landsat and PhenoCam imagery. Our results indicate that the VIIRS LSP product is very similar to the MODIS LCD product and can be used to extend the MODIS record, but some modest differences were found that users need to be aware of (and account for) if time series of VIIRS LSP and MODIS and LCD data are used together. In particular, we recommend that studies attempting to create long-term LSP time series by merging phenometrics from the MODIS LCD product with corresponding phenometrics from the VIIRS LSP product should estimate land cover-specific adjustments (i.e., following the basic procedure we used in this paper) that correct for modest systematic biases in the MODIS LCD product relative to the VIIRS LSP product.

Acknowledgments

This research was funded by NASA grant # NNX15AB96A ("Development and Validation of a Global Land Surface Phenology Product from NPP VIIRS for EOS-MODIS Continuity"). We thank the two anonymous reviewers for helping us improve the clarity of our research presentation.

Table A1
Number of valid and omitted pixels for the comparison between the VIIRS land surface phenology and MODIS land cover dynamics products. The values are stratified by the three dominant land cover types for each tile. IGBP land cover was derived from the collection 6 MODIS land cover type product: 4: deciduous broadleaf forests; 5: mixed forests; 7: open shrublands; 8: woody savannas; 9: savannas; 10: grasslands; 12: croplands.

Tile ID	IGBP	Product	Greenup onset			Date at mid-greenup			Maturity onset			Senescence onset			Date at mid-senescence			Dormancy onset			Average
			Valid	Omitted	%	Valid	Omitted	%	Valid	Omitted	%	Valid	Omitted	%	Valid	Omitted	%	Valid	Omitted	%	
Forests	5	VIIRS	1343732	8706	0.6	1343753	5795	0.4	1343927	14939	1.1	1342497	19348	1.4	1343732	4827	0.4	1343926	21473	1.6	0.9
		MODIS	1330320	22783	1.7	1330320	1690	0.1	1330320	3009	0.2	1330320	32602	2.5	1330320	942	0.1	1330320	13220	1.0	0.9
	4	VIIRS	1121600	4212	0.4	1121602	5377	0.5	1121614	8457	0.8	1121323	5395	0.5	1121600	4120	0.4	1121614	3205	0.3	0.5
		MODIS	1118929	6646	0.6	1118929	1042	0.1	1118929	3989	0.4	1118929	2205	0.2	1118929	67	0.0	1118929	2167	0.2	0.3
	8	VIIRS	818491	14891	1.8	818525	13600	1.7	818849	15566	1.9	815781	14756	1.8	818491	10837	1.3	818849	12044	1.5	1.7
		MODIS	809367	14628	1.8	809367	14331	1.8	809367	13917	1.7	809367	14339	1.8	809367	4912	0.6	809367	10279	1.3	1.5
Croplands	12	VIIRS	3027653	68593	2.3	3027653	41867	1.4	3027323	41295	1.4	3027352	48067	1.6	3027653	35809	1.2	3027323	38034	1.3	1.5
		MODIS	3013562	72532	2.4	3013562	66103	2.2	3013562	57210	1.9	3013562	78337	2.6	3013562	71784	2.4	3013562	70286	2.3	2.3
	8	VIIRS	650129	3696	0.6	650129	7479	1.2	650078	6672	1.0	650088	3934	0.6	650129	6888	1.1	650078	2726	0.4	0.8
		MODIS	632105	11513	1.8	632105	13569	2.1	632105	8521	1.3	632105	7099	1.1	632105	7016	1.1	632105	2819	0.4	1.3
	4	VIIRS	463973	2086	0.4	463973	1306	0.3	463973	1784	0.4	463973	344	0.1	463973	21	0.0	463973	27	0.0	0.2
		MODIS	463973	2086	0.4	463973	1306	0.3	463973	1784	0.4	463973	344	0.1	463973	21	0.0	463973	27	0.0	0.2
Shrublands/Grasslands	7	VIIRS	196104	6328	3.2	196104	7891	4.0	196104	7579	3.9	196104	2826	1.4	196104	6939	3.5	196104	2521	1.3	2.9
		MODIS	196104	6328	3.2	196104	7891	4.0	196104	7579	3.9	196104	2826	1.4	196104	6939	3.5	196104	2521	1.3	2.9
	10	VIIRS	486300	6625	1.4	486300	13330	2.7	486300	12514	2.6	486300	13467	2.8	486300	9308	1.9	486300	13490	2.8	2.4
		MODIS	486300	6625	1.4	486300	13330	2.7	486300	12514	2.6	486300	13467	2.8	486300	9308	1.9	486300	13490	2.8	2.4
	9	VIIRS	104981	746	0.7	104981	114	0.1	104981	118	0.1	104981	1236	1.2	104981	518	0.5	104981	657	0.6	0.5
		MODIS	104981	746	0.7	104981	114	0.1	104981	118	0.1	104981	1236	1.2	104981	518	0.5	104981	657	0.6	0.5
		Average	–	–	1.4	–	–	1.4	–	–	1.4	–	–	1.4	–	–	1.1	–	–	1.1	1.3

Table A2
Site information of the PhenoCam sites used in the study.

Camera name	Latitude (°)	Longitude (°)	Veg.	Full site name
Ahwahnee	37.7467	−119.5816	EN	Ahwahnee Meadow, Yosemite National Park, California
Arbutuslake	43.9821	−74.2332	DB	Arbutus Lake, Huntington Wildlife Forest, Newcomb, New York
Bartlettir	44.0646	−71.2881	DB	Bartlett Experimental Forest, Bartlett, New Hampshire
Boundarywaters	47.9467	−91.4955	DB	Boundary Waters Canoe Area Wilderness, Superior National Forest, Minnesota
Caryinstitute	41.7839	−73.7341	DB	Cary Institute of Ecosystem Studies, Millbrook, NY
Farewellgap	36.4530	−118.5900	EN	Farewell Gap/Mineral King, Sequoia National Park, California
Groundhog	48.2174	−82.1555	EN	Groundhog River, Ontario, Canada
Harvard	42.5378	−72.1715	DB	EMS Tower, Harvard Forest, Petersham, Massachusetts
Harvardbarn	42.5353	−72.1899	EN	Barn Tower, Camera 1, Harvard Forest, Petersham, Massachusetts
Harvardlph	42.5420	−72.1850	DB	LPH Tower, Harvard Forest, Petersham, Massachusetts
Hubbardbrook	43.9438	−71.7010	DB	Hubbard Brook Experimental Forest, USDA Forest Service Headquarters
Hubbardbrooknfws	42.9580	−71.7762	DB	North Facing Watersheds, Hubbard Brook Experimental Forest
Hubbardbrooksfws	43.9269	−71.7407	DB	South Facing Watersheds, Hubbard Brook Experimental Forest
Ibp	32.5890	−106.8470	GR	Jornada Experimental Range, New Mexico
Jasperridge	37.4020	−122.2210	GR	Jasper Ridge Biological Preserve, Woodside, California
Laurentides	45.9881	−74.0055	DB	Station de biologie des Laurentides, UniversityÂ of Montreal, Canada
Merbleue	45.4094	−75.5187	WL	Mer Bleue Conservation Area, Ottawa, Canada
Proctor	44.5250	−72.8660	DB	University of Vermont, Proctor Maple Research Center, Underhill, Vermont
Shalehillsczo	40.6500	−77.9000	DB	Susquehanna Shale Hills Critical Zone Observatory (CZO), Pennsylvania
Snakerivermn	46.1206	−93.2447	DB	Hay-Snake State Wildlife Management Area, near Woodland, Minnesota
Thompsonfarm2n	43.1086	−70.9505	DB	University of New Hampshire, Thompson Farm Observatory, Durham, New Hampshire
Tonzi	38.4309	−120.9659	DB	Tonzi Ranch, Amador County, California
Turkeypointdbf	42.6353	−80.5576	DB	Mature Deciduous Site, Turkey Point Carbon Cycle Research Project, Ontario, Canada
Turkeypointenf02	42.6609	−80.5595	EN	2002 White Pine, Turkey Point Carbon Cycle Research Project, Ontario, Canada
Turkeypointenf39	42.7098	−80.3574	EN	1939 White Pine, Turkey Point Carbon Cycle Research Project, Ontario Canada
Turkeypointenf74	42.7068	−80.3483	EN	1974 White Pine, Turkey Point Carbon Cycle Research Project, Ontario Canada
Twitchellalfalfa	38.1154	−121.6467	AG	Twitchell Island, Antioch, California, USA
Uiefmaize	40.0628	−88.1961	AG	Maize/Soybean agroecosystem at the University of Illinois Energy Farm
Uiefmiscanthus	40.0628	−88.1984	GR	Miscanthus agroecosystem at the University of Illinois Energy Farm
Uiefswitchgrass	40.0637	−88.1973	GR	Switchgrass agroecosystem at the University of Illinois Energy Farm
Umichbiological	45.5598	−84.7138	DB	University of Michigan Biological Station, near Pellston, Michigan
Vaira	38.4133	−120.9506	GR	Vaira Ranch, Amador County, California
Willowcreek	45.8060	−90.0791	DB	Willow Creek, Chequamegon-Nicolet National Forest, Wisconsin
Woodshole	41.5495	−70.6432	DB	Woods Hole Research Center, Falmouth, Massachusetts

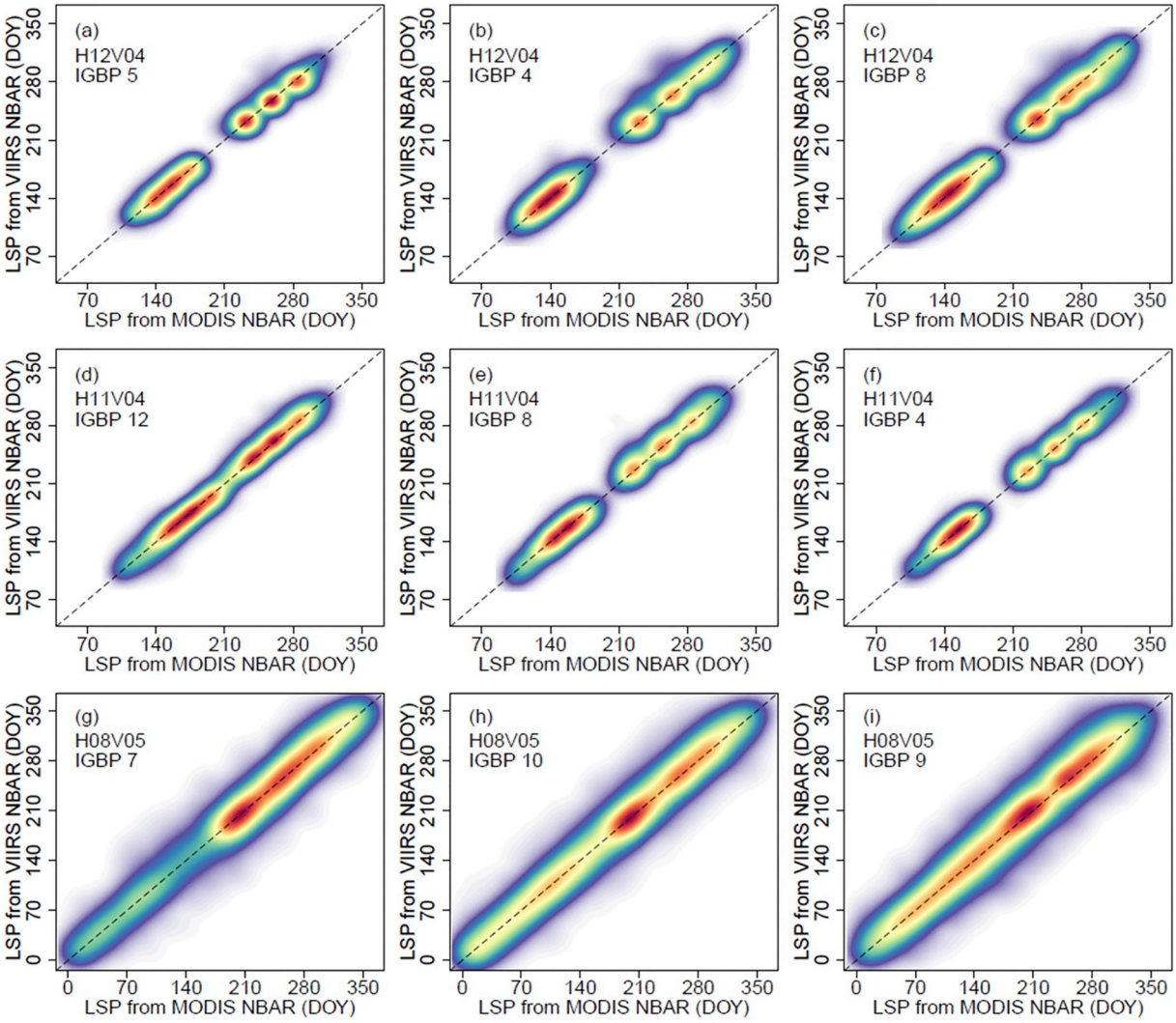

Fig. A1. Comparison of phenometrics retrieved from VIIRS and MODIS NBAR EVI2 time series using the VIIRS LSP algorithm in 2013, stratified by the three most common land cover types in each tile. IGBP land cover was derived from the Collection 6 MODIS Land Cover Type product: 4: deciduous broadleaf forests; 5: mixed forests; 7: open shrublands; 8: woody savannas; 9: savannas; 10: grasslands; 12: croplands. Red indicates high density and light purple indicates low density of observations. The dashed lines show 1:1 agreement.

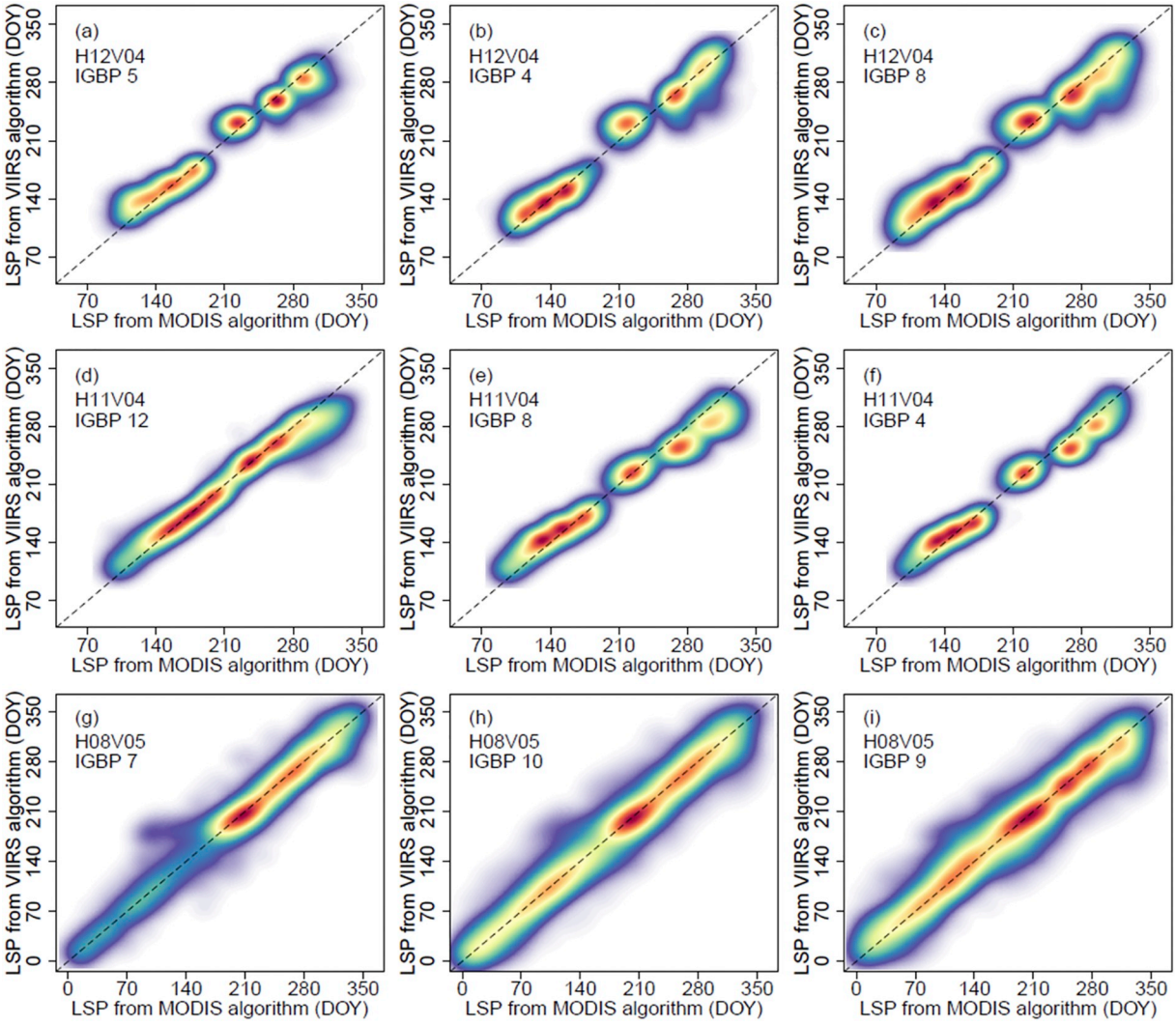

Fig. A2. Comparison of phenometrics retrieved from MODIS NBAR EVI2 time series using the VIIRS LSP and MODIS LCD algorithms in 2013, stratified by the three most common land cover types in each tile. IGBP land cover was derived from the Collection 6 MODIS Collection 6 Land Cover Type product: 4: deciduous broadleaf forests; 5: mixed forests; 7: open shrublands; 8: woody savannas; 9: savannas; 10: grasslands; 12: croplands. Red indicates high density and light purple indicates low density of observations. The dashed lines show 1:1 agreement.

References

de Beurs, K.M., Henebry, G.M., 2005. Land surface phenology and temperature variation in the international geosphere–biosphere program high-latitude transects. Glob. Chang. Biol. 11, 779–790. https://doi.org/10.1111/j.1365-2486.2005.00949.x.

Blanken, P.D., Black, T.A., 2004. The canopy conductance of a boreal aspen forest, Prince Albert National Park, Canada. Hydrol. Process. 18, 1561–1578. https://doi.org/10.1002/hyp.1406.

Buitenwerf, R., Rose, L., Higgins, S.I., 2015. Three decades of multi-dimensional change in global leaf phenology. Nat. Clim. Chang. 5, 364–368. https://doi.org/10.1038/nclimate2533.

Campagnolo, M.L., Sun, Q., Liu, Y., Schaaf, C., Wang, Z., Román, M.O., 2016. Estimating the effective spatial resolution of the operational BRDF, albedo, and nadir reflectance products from MODIS and VIIRS. Remote Sens. Environ. 175, 52–64. https://doi.org/10.1016/j.rse.2015.12.033.

Caprio, J.M., 1957. Phenology of lilac bloom in Montana. Science 126, 1344–1345. https://doi.org/10.1126/science.126.3287.1344.

Chen, M., Melaas, E.K., Gray, J.M., Friedl, M.A., Richardson, A.D., 2016. A new seasonal-deciduous spring phenology submodel in the community land model 4.5: impacts on carbon and water cycling under future climate scenarios. Glob. Chang. Biol. 22, 3675–3688. https://doi.org/10.1111/gcb.13326.

Dardel, C., Kergoat, L., Hiernaux, P., Mougin, E., Grippa, M., Tucker, C.J., 2014. Re-greening Sahel: 30 years of remote sensing data and field observations (Mali, Niger). Remote Sens. Environ. 140, 350–364. https://doi.org/10.1016/j.rse.2013.09.011.

Dorman, J.L., Sellers, P.J., 1989. A global climatology of albedo, roughness length and stomatal resistance for atmospheric general circulation models as represented by the simple biosphere model (SiB). J. Appl. Meteorol. 28, 833–855. https://doi.org/10.1175/1520-0450(1989)028<0833:AGCOAR>2.0.CO;2.

Efron, B., 1979. Bootstrap methods: another look at the jackknife. Ann. Stat. 7, 1–26. https://doi.org/10.1214/aos/1176344552.

Fang, J., Piao, S., Tang, Z., Peng, C., Ji, W., 2001. Interannual variability in net primary production and precipitation. Science 293, 1723. https://doi.org/10.1126/science.293.5536.1723a.

Fensholt, R., Rasmussen, K., 2011. Analysis of trends in the Sahelian 'rain-use efficiency' using GIMMS NDVI, RFE and GPCP rainfall data. Remote Sens. Environ. 115, 438–451. https://doi.org/10.1016/j.rse.2010.09.014.

Friedl, M.A., Gray, J.M., Melaas, E.K., Richardson, A.D., Hufkens, K., Keenan, T.F., Bailey, Amey, O'Keefe, J., 2014. A tale of two springs: using recent climate anomalies to characterize the sensitivity of temperate forest phenology to climate change. Environ. Res. Lett. 9, 054006. https://doi.org/10.1088/1748-9326/9/5/054006.

Ganguly, S., Friedl, M.A., Tan, B., Zhang, X., Verma, M., 2010. Land surface phenology from MODIS: characterization of the collection 5 global land cover dynamics product. Remote Sens. Environ. 114, 1805–1816. https://doi.org/10.1016/j.rse.2010.04.005.

Gray, J.M., Melaas, E.K., Sulla-Menashe, D., Moon, M., Friedl, M.A., 2019. Global Land Surface Phenology from MODIS: Collection 6 Products. (In Preparation).

Guay, K.C., Beck, P.S.A., Berner, L.T., Goetz, S.J., Baccini, A., Buermann, W., 2014. Vegetation productivity patterns at high northern latitudes: a multi-sensor satellite data assessment. Glob. Chang. Biol. 20, 3147–3158. https://doi.org/10.1111/gcb.12647.

Gutman, G.G., 1999. On the use of long-term global data of land reflectances and vegetation indices derived from the advanced very high resolution radiometer. J. Geophys. Res.: Atmos. 104, 6241–6255. https://doi.org/10.1029/1998JD200106.

Hogg, E.H., Price, D.T., Black, T.A., 2000. Postulated feedbacks of deciduous forest

phenology on seasonal climate patterns in the Western Canadian interior. J. Clim. 13, 4229–4243. https://doi.org/10.1175/1520-0442(2000)013<4229:PFODFP>2.0.CO;2.
Hufkens, K., Friedl, M., Sonnentag, O., Braswell, B.H., Milliman, T., Richardson, A.D., 2012. Linking near-surface and satellite remote sensing measurements of deciduous broadleaf forest phenology. Remote Sens. Environ. 117, 307–321. https://doi.org/10.1016/j.rse.2011.10.006.
Jiang, Z., Huete, A.R., Didan, K., Miura, T., 2008. Development of a two-band enhanced vegetation index without a blue band. Remote Sens. Environ. 112, 3833–3845. https://doi.org/10.1016/j.rse.2008.06.006.
Ju, J., Masek, J.G., 2016. The vegetation greenness trend in Canada and US Alaska from 1984–2012 Landsat data. Remote Sens. Environ. 176, 1–16. https://doi.org/10.1016/j.rse.2016.01.001.
Justice, C.O., Román, M.O., Csiszar, I., Vermote, E.F., Wolfe, R.E., Hook, S.J., Friedl, M., Wang, Z., Schaaf, C.B., Miura, T., Tschudi, M., Riggs, G., Hall, D.K., Lyapustin, A.I., Devadiga, S., Davidson, C., Masuoka, E.J., 2013. Land and cryosphere products from Suomi NPP VIIRS: overview and status. Journal of Geophysical Research: Atmospheres 118, 9753–9765. https://doi.org/10.1002/jgrd.50771.
Keenan, T.F., Gray, J., Friedl, M.A., Toomey, M., Bohrer, G., Hollinger, D.Y., Munger, J.W., O'Keefe, J., Schmid, H.P., Wing, I.S., Yang, B., Richardson, A.D., 2014. Net carbon uptake has increased through warming-induced changes in temperate forest phenology. Nat. Clim. Chang. 4, 598–604. https://doi.org/10.1038/nclimate2253.
Klosterman, S.T., Hufkens, K., Gray, J.M., Melaas, E., Sonnentag, O., Lavine, I., Mitchell, L., Norman, R., Friedl, M.A., Richardson, A.D., 2014. Evaluating remote sensing of deciduous forest phenology at multiple spatial scales using PhenoCam imagery. Biogeosciences 11, 4305–4320. https://doi.org/10.5194/bg-11-4305-2014.
Liang, L., Schwartz, M.D., Fei, S., 2011. Validating satellite phenology through intensive ground observation and landscape scaling in a mixed seasonal forest. Remote Sens. Environ. 115, 143–157. https://doi.org/10.1016/j.rse.2010.08.013.
Liu, Y., Wang, Z., Sun, Q., Erb, A.M., Li, Z., Schaaf, C.B., Zhang, X., Román, M.O., Scott, R.L., Zhang, Q., Novick, K.A., Syndonia Bret-Harte, M., Petroy, S., SanClements, M., 2017. Evaluation of the VIIRS BRDF, Albedo and NBAR products suite and an assessment of continuity with the long term MODIS record. Remote Sens. Environ. 201, 256–274. https://doi.org/10.1016/j.rse.2017.09.020.
Melaas, E.K., Friedl, M.A., Zhu, Z., 2013. Detecting interannual variation in deciduous broadleaf forest phenology using Landsat TM/ETM+ data. Remote Sens. Environ. 132, 176–185. https://doi.org/10.1016/j.rse.2013.01.011.
Melaas, E.K., Sulla-Menashe, D., Gray, J.M., Black, T.A., Morin, T.H., Richardson, A.D., Friedl, M.A., 2016. Multisite analysis of land surface phenology in north American temperate and boreal deciduous forests from Landsat. Remote Sens. Environ. 186, 452–464. https://doi.org/10.1016/j.rse.2016.09.014.
Menzel, A., Sparks, T.H., Estrella, N., Koch, E., Aasa, A., Ahas, R., Alm-Kübler, K., Bissolli, P., Braslavská, O., Briede, A., Chmielewski, F.M., Crepinsek, Z., Curnel, Y., Dahl, Å., Defila, C., Donnelly, A., Filella, Y., Jatczak, K., Måge, F., Mestre, A., Nordli, Ø., Peñuelas, J., Pirinen, P., Remišová, V., Scheifinger, H., Striz, M., Susnik, A., Vliet, A.J.H.V., Wielgolaski, F.-E., Zach, S., Zust, A., 2006. European phenological response to climate change matches the warming pattern. Glob. Chang. Biol. 12, 1969–1976. https://doi.org/10.1111/j.1365-2486.2006.01193.x.
Moore, K.E., Fitzjarrald, D.R., Sakai, R.K., Goulden, M.L., Munger, J.W., Wofsy, S.C., 1996. Seasonal variation in radiative and turbulent exchange at a deciduous forest in Central Massachusetts. J. Appl. Meteorol. 35, 122–134. https://doi.org/10.1175/1520-0450(1996)035<0122:SVIRAT>2.0.CO;2.
Nagol, J.R., Vermote, E.F., Prince, S.D., 2009. Effects of atmospheric variation on AVHRR NDVI data. Remote Sens. Environ. 113, 392–397. https://doi.org/10.1016/j.rse.2008.10.007.
Ollinger, S.V., Richardson, A.D., Martin, M.E., Hollinger, D.Y., Frolking, S.E., Reich, P.B., Plourde, L.C., Katul, G.G., Munger, J.W., Oren, R., Smith, M.-L., U, K.T.P., Bolstad, P. V., Cook, B.D., Day, M.C., Martin, T.A., Monson, R.K., Schmid, H.P., 2008. Canopy nitrogen, carbon assimilation, and albedo in temperate and boreal forests: functional relations and potential climate feedbacks. PNAS 105, 19336–19341. doi:https://doi.org/10.1073/pnas.0810021105.
Omernik, J.M., 1987. Ecoregions of the conterminous United States. Ann. Assoc. Am. Geogr. 77, 118–125. https://doi.org/10.1111/j.1467-8306.1987.tb00149.x.
Omernik, J.M., Griffith, G.E., 2014. Ecoregions of the conterminous United States: evolution of a hierarchical spatial framework. Environ. Manag. 54, 1249–1266. https://doi.org/10.1007/s00267-014-0364-1.
Park, T., Ganguly, S., Tømmervik, H., Euskirchen, E.S., Høgda, K.-A., Karlsen, S.R., Brovkin, V., Nemani, R.R., Myneni, R.B., 2016. Changes in growing season duration and productivity of northern vegetation inferred from long-term remote sensing data. Environ. Res. Lett. 11, 084001. https://doi.org/10.1088/1748-9326/11/8/084001.
Peñuelas, J., Rutishauser, T., Filella, I., 2009. Phenology feedbacks on climate change. Science 324, 887–888. https://doi.org/10.1126/science.1173004.
Richardson, A.D., Black, T.A., Ciais, P., Delbart, N., Friedl, M.A., Gobron, N., Hollinger, D.Y., Kutsch, W.L., Longdoz, B., Luyssaert, S., Migliavacca, M., Montagnani, L., Munger, J.W., Moors, E., Piao, S., Rebmann, C., Reichstein, M., Saigusa, N., Tomelleri, E., Vargas, R., Varlagin, A., 2010. Influence of spring and autumn phenological transitions on forest ecosystem productivity. Philosophical Transactions of the Royal Society of London B: Biological Sciences 365, 3227–3246. https://doi.org/10.1098/rstb.2010.0102.
Richardson, A.D., Keenan, T.F., Migliavacca, M., Ryu, Y., Sonnentag, O., Toomey, M., 2013. Climate change, phenology, and phenological control of vegetation feedbacks to the climate system. Agric. For. Meteorol. 169, 156–173. https://doi.org/10.1016/j.agrformet.2012.09.012.
Richardson, A.D., Hufkens, K., Milliman, T., Aubrecht, D.M., Chen, M., Gray, J.M., Johnston, M.R., Keenan, T.F., Klosterman, S.T., Kosmala, M., Melaas, E.K., Friedl, M.A., Frolking, S., 2018a. Tracking vegetation phenology across diverse North American biomes using PhenoCam imagery. Scientific Data 5, 180028. https://doi.org/10.1038/sdata.2018.28.
Richardson, A.D., Hufkens, K., Milliman, T., Frolking, S., 2018b. Intercomparison of phenological transition dates derived from the PhenoCam Dataset V1.0 and MODIS satellite remote sensing. Sci. Rep. 8, 5679. https://doi.org/10.1038/s41598-018-23804-6.
Ryu, Y., Baldocchi, D.D., Ma, S., Hehn, T., 2008. Interannual variability of evapotranspiration and energy exchange over an annual grassland in California. Journal of Geophysical Research: Atmospheres 113. https://doi.org/10.1029/2007JD009263.
Sakamoto, T., Wardlow, B.D., Gitelson, A.A., Verma, S.B., Suyker, A.E., Arkebauer, T.J., 2010. A two-step filtering approach for detecting maize and soybean phenology with time-series MODIS data. Remote Sens. Environ. 114, 2146–2159. https://doi.org/10.1016/j.rse.2010.04.019.
Schwartz, M.D., 1992. Phenology and springtime surface-layer change. Mon. Wea. Rev 120, 2570–2578. https://doi.org/10.1175/1520-0493(1992)120<2570:PASSLC>2.0.CO;2.
Sonnentag, O., Hufkens, K., Teshera-Sterne, C., Young, A.M., Friedl, M., Braswell, B.H., Milliman, T., O'Keefe, J., Richardson, A.D., 2012. Digital repeat photography for phenological research in forest ecosystems. Agric. For. Meteorol. 152, 159–177. https://doi.org/10.1016/j.agrformet.2011.09.009.
Sulla-Menashe, D., Woodcock, C.E., Friedl, M.A., 2018. Canadian boreal forest greening and browning trends: an analysis of biogeographic patterns and the relative roles of disturbance versus climate drivers. Environ. Res. Lett. 13, 014007. https://doi.org/10.1088/1748-9326/aa9b88.
Sulla-Menashe, D., Gray, J.M., Abercrombie, S.P., Friedl, M.A., 2019. Hierarchical mapping of annual global land cover 2001 to present: the MODIS collection 6 land cover product. Remote Sens. Environ. 222, 183–194. https://doi.org/10.1016/j.rse.2018.12.013.
Tan, B., Masek, J.G., Wolfe, R., Gao, F., Huang, C., Vermote, E.F., Sexton, J.O., Ederer, G., 2013. Improved forest change detection with terrain illumination corrected Landsat images. Remote Sens. Environ. 136, 469–483. https://doi.org/10.1016/j.rse.2013.05.013.
Verma, M., Friedl, M.A., Finzi, A., Phillips, N., 2016. Multi-criteria evaluation of the suitability of growth functions for modeling remotely sensed phenology. Ecol. Model. 323, 123–132. https://doi.org/10.1016/j.ecolmodel.2015.12.005.
White, M.A., Beurs, K.M.D., Didan, K., Inouye, D.W., Richardson, A.D., Jensen, O.P., O'keefe, J., Zhang, G., Nemani, R.R., Leeuwen, W.J.D.V., Brown, J.F., Wit, A.D., Schaepman, M., Lin, X., Dettinger, M., Bailey, A.S., Kimball, J., Schwartz, M.D., Baldocchi, D.D., Lee, J.T., Lauenroth, W.K., 2009. Intercomparison, interpretation, and assessment of spring phenology in North America estimated from remote sensing for 1982–2006. Glob. Chang. Biol. 15, 2335–2359. https://doi.org/10.1111/j.1365-2486.2009.01910.x.
Yang, X., Tang, J., Mustard, J.F., 2014. Beyond leaf color: comparing camera-based phenological metrics with leaf biochemical, biophysical, and spectral properties throughout the growing season of a temperate deciduous forest. Journal of Geophysical Research: Biogeosciences 119, 181–191. https://doi.org/10.1002/2013JG002460.
Zhang, X., 2015. Reconstruction of a complete global time series of daily vegetation index trajectory from long-term AVHRR data. Remote Sens. Environ. 156, 457–472. https://doi.org/10.1016/j.rse.2014.10.012.
Zhang, X., Friedl, M.A., Schaaf, C.B., Strahler, A.H., Hodges, J.C.F., Gao, F., Reed, B.C., Huete, A., 2003. Monitoring vegetation phenology using MODIS. Remote Sens. Environ. 84, 471–475. https://doi.org/10.1016/S0034-4257(02)00135-9.
Zhang, X., Friedl, M.A., Schaaf, C.B., Strahler, A.H., 2004. Climate controls on vegetation phenological patterns in northern mid- and high latitudes inferred from MODIS data. Glob. Chang. Biol. 10, 1133–1145. https://doi.org/10.1111/j.1529-8817.2003.00784.x.
Zhang, X., Friedl, M.A., Schaaf, C.B., 2006. Global vegetation phenology from Moderate Resolution Imaging Spectroradiometer (MODIS): evaluation of global patterns and comparison with in situ measurements. J. Geophys. Res.: Biogeosci. 111. https://doi.org/10.1029/2006JG000217.
Zhang, X., Liu, L., Yan, D., 2017a. Comparisons of global land surface seasonality and phenology derived from AVHRR, MODIS, and VIIRS data. J. Geophys. Res.: Biogeosci. 122, 1506–1525. https://doi.org/10.1002/2017JG003811.
Zhang, X., Wang, J., Gao, F., Liu, Y., Schaaf, C., Friedl, M., Yu, Y., Jayavelu, S., Gray, J., Liu, L., Yan, D., Henebry, G.M., 2017b. Exploration of scaling effects on coarse resolution land surface phenology. Remote Sens. Environ. 190, 318–330. https://doi.org/10.1016/j.rse.2017.01.001.
Zhang, X., Jayavelu, S., Liu, L., Friedl, M.A., Henebry, G.M., Liu, Y., Schaaf, C.B., Richardson, A.D., Gray, J., 2018a. Evaluation of land surface phenology from VIIRS data using time series of PhenoCam imagery. Agric. For. Meteorol. 256–257, 137–149. https://doi.org/10.1016/j.agrformet.2018.03.003.
Zhang, X., Liu, L., Liu, Y., Jayavelu, S., Wang, J., Moon, M., Henebry, G.M., Friedl, M.A., Schaaf, C.B., 2018b. Generation and evaluation of the VIIRS land surface phenology product. Remote Sens. Environ. 216, 212–229. https://doi.org/10.1016/j.rse.2018.06.047.
Zhao, L., Lee, X., Suyker, A.E., Wen, X., 2016. Influence of leaf area index on the radiometric resistance to heat transfer. Boundary-Layer Meteorol 158, 105–123. https://doi.org/10.1007/s10546-015-0070-4.